

The temporal and spatial characteristics of TOPEX/POSEIDON radial orbit error

J.A. Marshall

Space Geodesy Branch, NASA Goddard Space Flight Center, Greenbelt, Maryland

N.P. Zelensky, S.M. Klosko, D.S. Chinn, S.B. Luthcke, K.E. Rachlin

and R.G. Williamson

Hughes STX Corporation, Greenbelt, Maryland

Abstract. Satellite orbit error has long been the bane of oceanographers who analyze altimetry data. However, radial orbit error on TOPEX/POSEIDON (T/P) has been reduced to the 3 to 4-cm root-mean-square (rms) level over a 10-day repeat cycle, which represents an order of magnitude improvement over earlier altimetry missions such as Geosat. Consequently, oceanographers are now able to directly evaluate the absolute ocean topography to unprecedented accuracy levels. While significantly reduced, the T/P orbit error still requires quantification. This study examines the spatial and temporal characteristics of the T/P radial orbit error, as assessed through the analysis of laser tracking residuals and orbit comparisons with independently generated trajectories. Spectral analyses of the orbit differences between the orbits determined from satellite laser ranging and Doppler Orbitography and Radiopositioning Integrated by Satellite data and the independently determined reduced dynamic Global Positioning System (GPS) ephemerides indicate that the predominant power is at the once-per-orbital revolution frequency with 2- to 3-cm peaks. When the orbit differences are colinearly aligned to a fixed geographic grid and spectral analysis is performed at each geographic grid point, a nearly 60-day period is found with maximum amplitudes in the 2- to 4-cm range. The contribution of both conservative and nonconservative force and measurement mismodeling to this error signal are assessed. We demonstrate that the ~60-day error period seen at fixed geographic locations arises from weaknesses in the dynamic ocean tidal models used in the orbit calculations. New tidal models have been developed which significantly reduce this error. Second-generation orbits incorporating many model improvements have been computed and demonstrate a significant reduction in the radial orbit error signals. Some orbit error still exists, and methods for further model improvements and the possibility of achieving 1-cm radial rms orbit accuracy in T/P are discussed.

1. Introduction

Satellite altimetry has provided the oceanographic community with a global synoptic observational data set of the ocean surface topography and, when combined with knowledge of the geoid, the major geostrophic currents. In the past, insufficient knowledge of the spacecraft's radial position has limited the application of these data sets. Seasat radial positioning accuracy was estimated to be 1.5 m [Marsh and Williamson, 1980; Schutz and Tapley, 1980], and Geosat was between 25 and 85 cm, depending upon the gravity field used [Haines *et al.*, 1990, 1994]. Consequently, investigators developed empirical strategies to remove the orbit error from the altimetric data at the expense of losing valid long-wavelength oceanographic signal [Cheney *et al.*, 1983]. These techniques, however, have proved unnecessary and provide degraded oceanographic results when analyzing the TOPEX/POSEIDON (T/P) altimetry data using the precise orbits on the mission geophysical data records (GDRs).

The T/P satellite flies in a nearly circular orbit at an average altitude of 1336 km with an inclination of 66.05°. It has a period of

112.4 min and a ground track repeat cycle of 9.9156 days after completing 127 orbital revolutions. The rate of change for the argument of perigee is near zero in order to satisfy the "frozen" repeat orbit criteria. Orbit maintenance maneuvers are performed about every 3 months to keep the orbit ground track repeating to within ± 1 km and the mean orbit eccentricity near zero. The rms radial orbit errors for T/P are between 3 and 4 cm due largely to improved gravity and nonconservative force models [Nerem *et al.*, 1994; Tapley *et al.*, 1994a]. However, even orbit errors of this small magnitude can adversely affect certain altimeter applications and need to be understood. Accordingly, the purpose of this paper is to assess the temporal and spatial characteristics of the T/P radial orbit error, identify possible sources for the error, and explore strategies for reducing or eliminating their effect.

The fact that no measure of absolute orbit accuracy exists makes the process of assessing orbit quality difficult. Several different methods are used to infer orbit accuracy; these include agreement with the tracking data, orbit overlap tests generated from subsets of the tracking data, and orbit comparisons with independently computed ephemerides. No single test directly measures the complete orbit error, but as an aggregate, they can provide a reasonable estimate. For past altimetric missions the altimeter range and crossover residuals were widely used as an independent measure to quantify errors in the satellite's radial position. However, for this T/P study, mesoscale sea surface variations, uncertainty in modeling ocean

Copyright 1995 by the American Geophysical Union.

Paper number 95JC01845.
0148-0227/95/95JC-01845\$05.00

tides, and geoid errors are all large compared to the residual orbit error. Fortunately, T/P carries four independent tracking data systems: satellite laser ranging (SLR), Doppler Orbitography and Radiopositioning Integrated by Satellite (DORIS), Global Positioning System (GPS) demonstration receiver, and the Tracking and Data Relay Satellite System (TDRSS). A comparison of ephemerides generated from these different tracking types provides a unique opportunity to assess the radial orbit error contained in the T/P orbits.

A traditional dynamic orbit determination methodology is used to compute the precise orbit ephemeris (POE) found on the mission GDRs from the SLR and DORIS measurements. This approach is dependent upon and inherently limited by detailed modeling of the complete set of forces acting on the T/P spacecraft as well as all components of and corrections to the tracking measurements [Marshall and Luthcke, 1994a, b; Nerem et al., 1993, 1994; Tapley et al., 1994a].

An experimental GPS receiver was flown as a demonstration of its satellite-to-satellite tracking capabilities and has yielded orbit accuracies comparable to those obtained from SLR/DORIS [Bertiger et al., 1994; Yunck et al., 1990]. The dense temporal and three-dimensional spatial coverage of this data type permits the use of a reduced dynamic orbit determination strategy. In the GPS reduced dynamic approach, residual dynamic force modeling error is significantly reduced [Wu et al., 1991; Yunck et al., 1990, 1994]. However, accurate GPS satellite positions, antenna phase center locations, and an appropriate reference frame realization are all potential error sources for the reduced dynamic approach. Consequently, while still imperfect, the reduced dynamic ephemerides produced from the GPS data are likely to have errors which differ in character from those found within the NASA SLR/DORIS POEs and will provide a measure of POE errors.

Sections 2 and 3 of this paper examine the potential contributions of conservative and nonconservative force model errors, respectively, to the observed orbit error signal. Section 4 investigates the effect of measurement model errors. A detailed description of the temporal and spatial characteristics of the differences between the SLR/DORIS and GPS orbits is presented in section 5. Because of their independent nature, comparisons of the SLR/DORIS and GPS determined ephemerides are used as a calibration of orbit error. SLR data provide the most accurate and least ambiguous measurement of orbit position on an observation-by-observation basis. Therefore additional analysis of the laser residuals are used to augment the orbit difference results and to provide the necessary link to the absolute orbit error. Finally, section 6 presents an error budget for both the first- and second-generation orbits and explores the improvements necessary to meet a ± 1 -cm radial accuracy goal for T/P.

2. Gravity and Tide Model Errors

Gravity (static and variable) modeling improvements in support of the TOPEX/POSEIDON project began at Goddard Space Flight Center in 1983. Error covariance studies performed at that time on Goddard Earth Model (GEM)-L2 [Lerch et al., 1982] revealed gravity modeling improvements of about 1 order of magnitude were required to meet the 10-cm radial accuracy goals of T/P. Over the ensuing decade, several gravity models of progressively improved quality were developed using improved data analysis techniques and ancillary models. These efforts culminated in a pre-launch Joint Gravity Model (JGM)-1 and postlaunch JGM-2 [Nerem et al., 1994]. JGM-2 incorporates SLR and DORIS data

obtained during the first 15 10-day cycles to "tune" the field for T/P-specific effects and is used when producing the POEs. Similarly, four cycles of GPS and eight additional cycles of SLR/DORIS tracking data of T/P were added to the JGM-2 gravity field solution to produce JGM-3 [Tapley et al., 1994b]. The ocean tidal model used in these first generation orbit computations was based on a combination of the Schwiderski [1983] oceanographic models, solutions for long-wavelength terms using satellite tracking data, and application of linear admittances to effectively model all T/P-sensitive tidal constituents to a level sufficient to meet mission requirements. Error characteristics of both the gravity and tide models are discussed in detail below.

2.1. Orbit Errors From the Static Gravitational Field

The radial errors induced when computing a near-Earth orbital ephemeris from an imperfect gravity model is an area that has received considerable study over the last decade [e.g., Tapley and Rosborough, 1985; Colombo, 1986; Wagner, 1987; Rosborough and Tapley, 1987; Schrama, 1992; Lerch et al., 1993a, b; Chelton and Schlax, 1993; Nerem et al., 1993, 1994; Tapley et al., 1994a, b]. While it is beyond the scope of this paper to extensively review these studies, it is nevertheless important to give an overall characterization of the radial errors predicted for T/P based on the calibrated error covariance of the JGM-2 field.

Using linear orbit perturbation theory [Kaula, 1966], the gravitational field produces errors that are periodic at frequencies

$$\dot{\psi} = (n - 2p + q)(\dot{M} + \dot{\omega}) - q\dot{\omega} + m(\dot{\Omega} - \dot{\theta}) \quad (1)$$

where

- n degree of the Stokes harmonics;
- m order of the Stokes harmonics;
- p subscript in the inclination function;
- q subscript in the eccentricity function;
- $\dot{\omega}$ mean rate of the argument of perigee;
- $\dot{\Omega}$ mean node rate;
- \dot{M} mean anomalistic motion rate;
- $\dot{\theta}$ mean rotation rate of the Earth.

For near-circular orbits like T/P the range of subscripts of concern are as follows: n , from 2 to 70; m , from 0 to 70; q , = 0, ± 1 , ± 2 ; and p ranges from 1 to n . Allowing $k = (n - 2p + q)$, the dominant errors from the gravity field have frequencies of

$$k \text{ cycles/revolution} \pm m \text{ cycles/day} \quad (2)$$

For a near-circular satellite orbit with a repeating ground track in which the argument of perigee is "frozen," as is typical for altimeter satellites, Kaula's [1966] linear orbit perturbation theory demonstrates that the gravitational field produces a complicated error spectrum with the majority of the signal occurring at or near one cycle-per-orbital revolution (1 cpr). This is also the dominant frequency for nonconservative force model errors discussed in section 3. The classes of orbit perturbation frequencies arising from gravity field error are summarized in Table 1. The orbit error arising from the gravity model can be segregated into time-invariant and time varying components [e.g., Tapley and Rosborough, 1985; Engelis, 1985; Wagner, 1985; Melvin, 1988]. All such error is a function of geographic position. Those that are time invariant are not dependent upon the direction of the satellite's motion. Those that are time varying produce errors that change sign, depending on whether the satellite is on an ascending or descending pass. The gravity portion of the difference between the ascending and descending errors at the

Table 1. Gravity Field Induced Orbit Perturbations

Breakdown by Index k =	Rate Arguments	Classification
0	$\psi \approx m\theta$	m daily
$m = 0$	$\psi \approx q\dot{\omega}$	long period
0	$kM \approx m\dot{\theta}$	short period
1, 2, 3	$kM \approx m\dot{\theta}$	resonant

altimeter crossover point remains constant for each repeat cycle and is commonly referred to as "geographically correlated" orbit error. As a rule of thumb, the variance of this error is ~50% of the variance of the total radial error due to gravity [Rosborough and Tapley, 1987]. At periods longer than an orbital revolution, errors in the resonance and odd zonal harmonics of the gravity model produce modulation of the 1 cpr error amplitude over the orbital arc length. As a result, within the least squares orbit estimation environment, 1 cpr orbit errors appear to grow as a function of time from the middle of the arc. This is the so-called "bow-tie" error effect described by Colombo [1986].

The power spectra of the T/P radial orbit error have been derived from the JGM-2 covariance through use of a related model called a "clone" (see Nerem *et al.* [1993] for the methodology to compute a clone of a given field). A clone of a given model deviates from the original by 1 fully correlated standard deviation and is one example in an infinite number of such models that can be used for Monte Carlo testing procedures. The T/P radial orbit differences between using JGM-2 and its clone have been spectrally analyzed giving the amplitude spectrum shown in Figure 1. Much of the field differences produce errors at the modulating frequencies of 1 cpr plus/minus 1 and 2 cycles per day (cpd). This amplitude spectrum will be compared to observed orbital effects in section 5.

JGM-2 error covariance propagation studies indicate a radial rms error of 2.2 cm is expected on T/P from gravity field mismodeling, of which 1.6 cm is geographically correlated. The geographic distribution of the correlated orbit error is shown in Plate 1. The largest spatially coherent pattern seen in Plate 1 can be described as a $P_{1,1}$ surface harmonic (with evenly spaced hemispheric highs and lows along the equator). This pattern characteristically arises from errors in order one, odd degree terms in the gravity field which are associated with radial errors having 1 cpr \pm 1 cycle-per-day (1 cpd) periods coming from the m -daily orbit element perturbations of the first-order harmonics. While smaller structure is observable in Plate 1, it is of little apparent consequence compared with the 1 cpd effects.

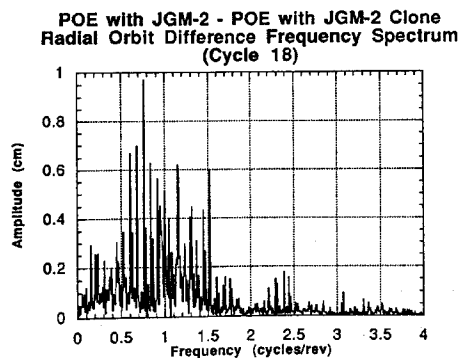


Figure 1. Amplitude spectrum of radial orbit difference between Joint Gravity Model (JGM-2) and JGM-2 clone (cycle 18).

2.2. Earth and Ocean Tide Model Errors

As orbit accuracy requirements have grown more stringent, the need to address the orbit perturbations arising from long-wavelength solid Earth and ocean tides has risen in importance. Bettadpur and Eanes [1994] have shown that limiting orbit errors induced by tide model errors are especially important for those trying to improve ocean tide models from T/P altimetry data, since the tide model errors manifest themselves in both the orbit and ocean with similar spectra. In recent geopotential solutions it has been a common practice to simultaneously recover spherical harmonic terms in the tidal expansion for major tidal constituents, [Marsh *et al.*, 1988, 1990; Christodoulidis *et al.*, 1988; Lerch *et al.*, 1994a; Cheng *et al.*, 1990]. Nerem *et al.* [1993, 1994] summarize the tide modeling techniques used to achieve the accuracy required for T/P. Specifically, the long-wavelength tidal terms that are in resonance with near-Earth satellites give rise to sizable long-period perturbations, thus allowing their determination from satellite tracking data. The short-period orbital perturbations from tides are modeled by a large number of tidal coefficients spanning many tide lines based on tide models developed from oceanographic data (tide gauges, satellite altimetry) and hydrodynamic modeling. This latter part comprises the background ocean tide model. The ocean tide model is applied in the presence of a frequency-dependent model of the solid Earth tides developed by Wahr [1979, 1981]. The tidal solution from the tracking data is made in the space of the ocean tides because this model is more uncertain than that of the solid Earth. However, each tidal term that is estimated accommodates ocean, atmospheric, and solid Earth mass redistribution at a specified astronomic frequency.

Many tidal components, while being diurnal or semidiurnal on the Earth's surface (due to the Earth's rotation with respect to the Sun and Moon), give rise to long-period orbital resonance perturbations (see Table 2). The complete tide model from recent solutions contains both adjusted (resonance) and unadjusted (short period) terms. The solid Earth tides are assumed to have a zero phase angle and are therefore free of dissipation. However, any residual phase due to anelastic properties of the solid Earth are accounted for in the adjusted subset of terms. We have adjusted terms for the 12 major tidal frequencies [Lerch *et al.*, 1994]. The resulting model from these solutions reflects the external tidal potential sensed by Earth-orbiting satellites arising from the tidal redistribution of mass in the integrated solid Earth/ocean/atmosphere systems.

The long-period tidal terms in resonance with the T/P orbit produce the largest perturbations. The introduction of extensive and frequent empirical acceleration adjustment as part of the T/P POE strategy assures a great degree of accommodation for errors made in modeling the long-period resonance tidal perturbations. For example, while the Centre National d'Etudes Spatiales (CNES) and NASA Precise Orbit Determination (POD) groups used quite different resonance tidal models, the resulting ephemerides agree at the 1- to 2-cm level rms in the radial direction [Noel *et al.*, 1994]. It is predominantly the background tidal model, which contains both omission and commission errors, that gives rise to short-period orbit perturbations and now warrants the most scrutiny. These errors are not effectively removed within the dynamic orbit determination strategy used to produce the POEs.

The background tide model was developed based on the analysis of Casotto [1989], who used an analytical orbit theory to evaluate the ocean tidal perturbations on the T/P orbit. A set of spherical harmonic coefficients for over 80 tide lines was identified as important for T/P. Many of these are sideband tides, and some are tides that result from the interaction of the third bodies with one another. These latter tides are implicitly modeled in our GEODYN formula-

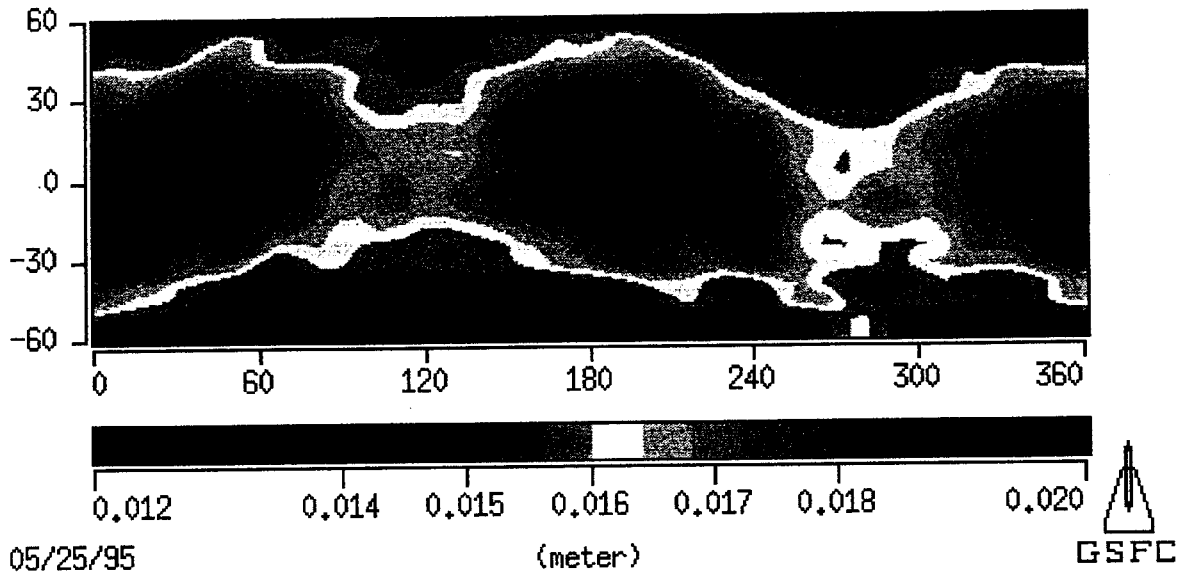


Plate 1. Geographically correlated orbit error as predicted by JGM-2 covariance.

tion through the use of the osculating Kepler elements of the perturbing bodies [Rowlands *et al.*, 1994]. Consult Nerem *et al.* [1993] for a discussion of the adopted background tide model, testing for the level of omission errors, and a listing of the complete set of tidal constituents included in the model. The goal for the background model design was to keep omission errors from the ocean tides to less than 1 cm root-sum-square (rss) radially on the T/P orbit. The resulting background tide model has over 1600 coefficients selected among the dominant tides, and if one includes the total size of the model considering evaluation of all the terms contained within each of the tidal families, more than 6000 terms are being modeled. This is the a priori background ocean tidal model which is used for the first generation NASA T/P POE.

The magnitude of the short-period orbit error is roughly a function of the tidal mismodeling at the subsatellite point. These orbit errors are largest when and where the tide model is most in error and have the same aliasing period (described in Table 2) as that of the tidal sampling itself. The theoretical bases for these perturbations are given by Colombo [1984] and Bettadpur and Eanes [1994].

For the adopted background model the omission error on the radial component of the T/P orbit was estimated to be 0.8 cm [Nerem *et al.*, 1993]. For this paper, augmented background tide models have been developed and tested based on improved tide models developed from the T/P altimetry by Ray *et al.* [1994]. These models include M_2 , S_2 , N_2 , K_2 , P_1 , O_1 , Q_1 , and K_1 harmonic

Table 2. Comparison of Tidal Periods on Earth's Surface, Corresponding Resonance Orbit Perturbation Period, and Aliasing Period

Tidal Constituent	Period on Earth's Surface	Resonance Period for TOPEX/POSEIDON Orbit Perturbations, days	TOPEX/POSEIDON Aliasing Period, days ^a
S_a 056.5545	1.0139 years	same	same
S_{sa} 057.5555	182.62 days	same	same
M_m 065.4555	27.55 days	same	same
M_f 075.5555	13.66 days	same	36.2
Q_1 135.6555	1.120 days	86.8	69.4
O_1 145.5555	1.076 days	12.7	45.7
P_1 163.5555	1.003 days	89.0	88.9
K_1 165.5555	23.935 hours	174	173.2
\emptyset_1 167.5535	23.805 hours	3,580	329.4
N_2 245.6555	12.658 hours	8.26	49.5
M_2 255.5555	12.421 hours	11.8	62.1
S_2 273.5555	12.000 hours	58.9	58.7
K_2 275.5555	11.967 hours	86.9	86.6

^aAliasing period is to sample complete tidal cycle at a fixed point on the Earth's surface.

models complete to degree and order 15 and are significantly advanced over those available from Schwiderski [1983]. Analysis associated with these improved tidal models is introduced in the section 5 to quantify the effect of tidal omission and commission errors.

3. Nonconservative Force Modeling

In order to meet the stringent orbit accuracies required for the T/P mission, it was no longer adequate to treat the spacecraft as a homogeneous sphere in the orbit determination process. Therefore an exhaustive effort to characterize T/P's shape, attitude, material properties, and acceleration history was undertaken [Antreasian and Rosborough, 1992; Marshall and Luthcke, 1994a, b]. From these investigations the spacecraft was modeled as a set of eight flat plates arranged in the shape of a box and connected wing. Each plate possesses its own properties (area, specular and diffuse reflectivity, emissivity, and temperature) which represent the aggregate composition of the components comprising each side of the spacecraft. The nonconservative forces acting on each flat plate (i.e., solar radiation, albedo, thermal imbalance, atmospheric drag) are computed independently and then summed to produce the overall acceleration on the spacecraft center of mass. Prelaunch values for the plate parameters were derived from the result of the finite element analysis. This "macromodel" was tuned simultaneously with the gravity model using the first 15 cycles of T/P SLR and DORIS tracking data to better reflect the observed behavior. The model has demonstrated excellent performance, accounting for over 95% of the observed accelerations [Marshall and Luthcke, 1994b]. The residual nonconservative forces are largely accounted for through the adjustment of daily empirical accelerations [Tapley et al., 1994a].

Nonetheless, nonconservative force mismodeling remains a major contributor to the current T/P orbit errors. To better understand this contribution and identify possible improvements, several assumptions implicit in developing the macromodel have been further examined and tested using on-orbit T/P telemetered data. These include an assessment of the attitude model, the solar array temperature algorithm, and evidence of material property degradation. Also, the parameterization and recovered values of the empirical accelerations are examined for indications of orbit error based on their behavior with regards to Sun/satellite geometry and attitude events.

3.1. Attitude Analysis

The T/P spacecraft follows a complicated yaw-steering attitude control algorithm to facilitate optimal Sun pointing of the solar array given constraints on the responsiveness of the solar array drives. This involves rotation about the nadir-pointing axis within four different yaw regimes: fixed, ramp, sinusoidal, and flip. In fixed yaw, no rotation occurs. In sinusoidal yaw, the yaw angle increases and decreases according to a sinusoidal algorithm. Yaw ramp is the transition between fixed and sinusoidal. Yaw flip involves a 180° rotation over half of an orbital revolution. Proper modeling of the complicated attitude control law is necessary for both precise force and measurement modeling. Much of the complicated attitude control algorithm is currently being modeled in the evaluation of the T/P macromodel [Marshall and Luthcke, 1994a]. However, certain simplifications have been made that produce attitude modeling errors. Currently, the spacecraft flip is modeled as instantaneous, and no roll, pitch, or yaw biases are considered beyond the deliberate pitch bias introduced for the solar array. These are the known modeling errors, and, in reality, there may, of course, be others. For-

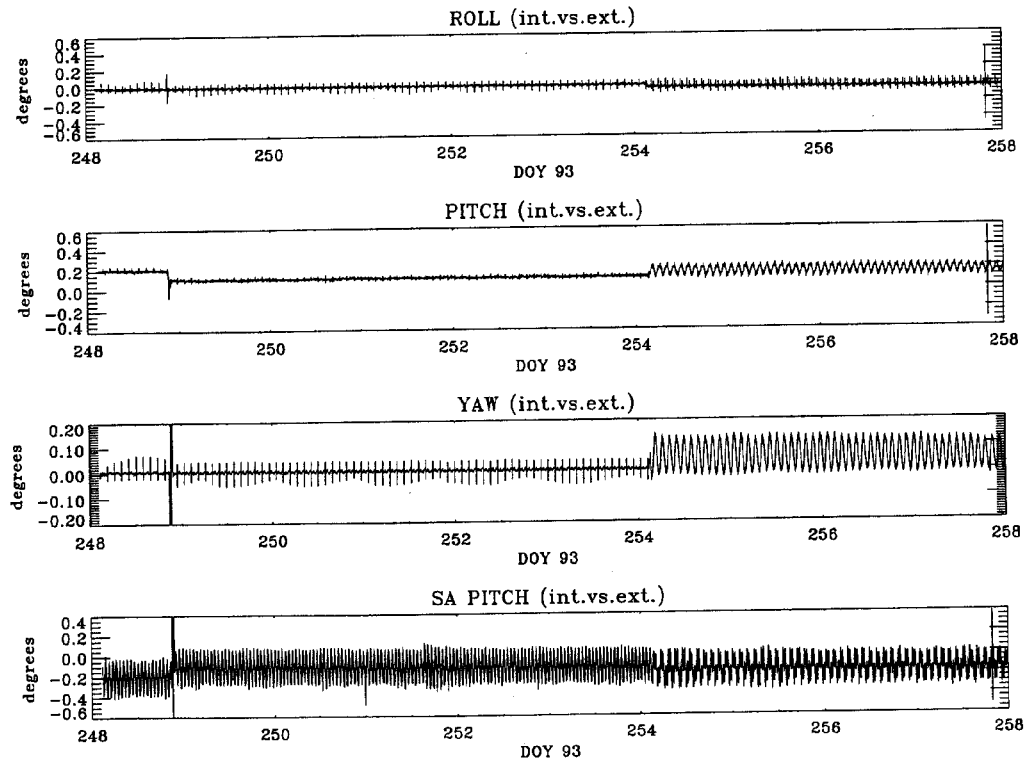


Figure 2. Computed versus measured TOPEX/POSEIDON (T/P) attitude.

Table 3. Attitude Differences for Cycle 36 (Internal Model Versus Telemetered Attitude)

Regime	Body Roll		Body Pitch		Body Yaw		SA Pitch	
	Mean	Standard Deviation	Mean	Standard Deviation	Mean	Standard Deviation	Mean	Standard Deviation
Fixed	-0.89	0.87	10.84	0.60	0.66	0.64	-11.27	9.92
Sinusoidal	-4.12	1.17	15.64	3.49	5.45	5.04	-15.44	8.75

All values are 10^{-2} degrees. SA is solar array.

tunately, a direct comparison between the modeled attitude and the telemetered spacecraft attitude data can be used to understand and evaluate the impact of these assumptions.

The capability to ingest telemetered attitude has been incorporated into the GEODYN orbit determination software in order to accommodate off-nominal attitude events [Rowlands *et al.*, 1994]. The telemetered attitude information contains spacecraft body and solar array (SA) quaternions measured by the onboard star trackers at 8-s intervals which describe the attitude of the spacecraft (S/C) with respect to the inertial frame. In this study the difference between the modeled and telemetered quaternions is evaluated in terms of roll, pitch, and yaw. The orbit ephemeris derived using the standard modeled attitude is differenced with its counterpart computed from telemetered quaternions. Analysis of SLR and DORIS measurement residuals are also used to gauge the attitude performance.

Cycle 36 incorporates all attitude regimes, including both a ramp and a flip. Figure 2 shows the time series of the internal and telemetered S/C body and SA attitude differences, respectively, in the spacecraft roll, pitch, and yaw directions. Note that the SA only

rotates about the pitch axis, and the roll and yaw differences are consequently zero. The largest internal attitude modeling error for this cycle occurs at day 248.8 during the yaw flip. This is expected, since the flip event is treated as an instantaneous transition (from 0 to 180, or 180 to 0° yaw) within the macromodel code. During this 60-min event the attitude modeling error reaches 95° in the S/C-body yaw and 9° in the SA pitch. A yaw ramp occurs near day 254.2 and exhibits no significant modeling errors in either the S/C body and SA attitude. Overall, the internal attitude model properly mimics the actual attitude of the S/C body to 0.05° standard deviation (s.d.) about the mean over the 10-day cycle (excluding flip) and 0.09° s.d. for the SA pitch (again, excluding flip). The mean difference can be as large as 0.15° for the S/C body and SA pitch during sinusoidal yaw steering. Additional relevant statistics are displayed in Table 3.

Note that Figure 2 and Table 3 both demonstrate a significant change in attitude error characteristics, depending on the yaw regime. Spectral analysis shows that during the fixed yaw regime, the S/C-body roll and yaw error exhibits power at primarily a 1 and 2 cpr, while the S/C body and SA pitch exhibit a primarily 2 cpr sig-

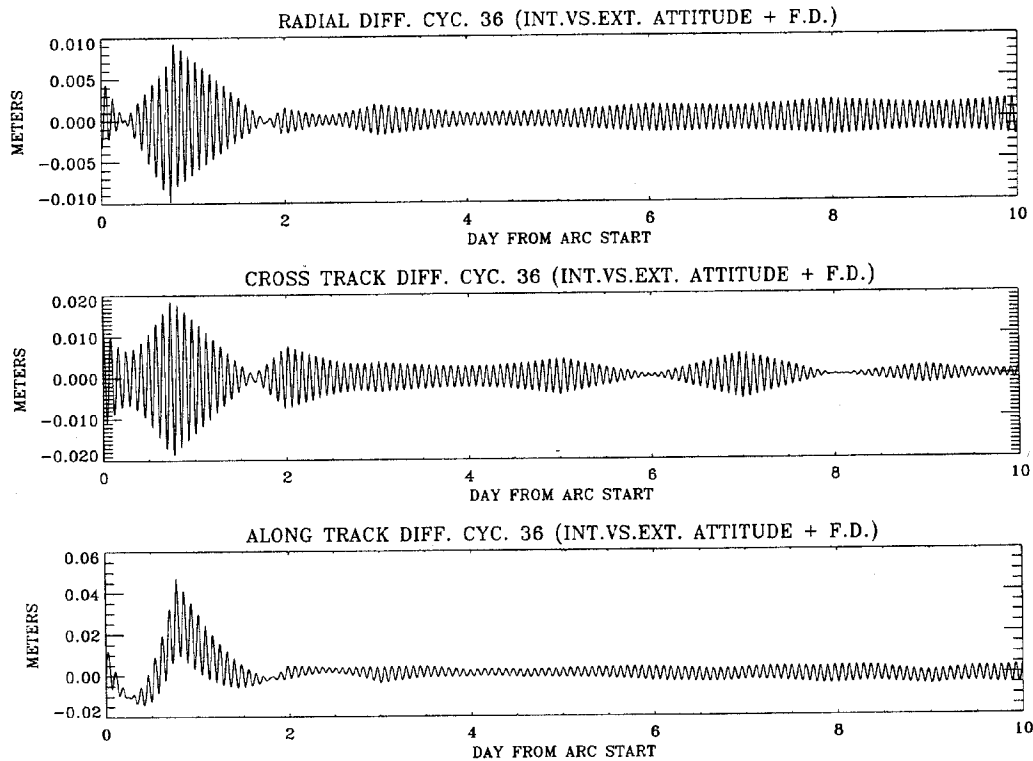


Figure 3. T/P orbit error between computed and measured T/P attitude.

Table 4. Orbit Differences for Cycle 36
(Internal Model Versus Telemetered Attitude)

Component	rms	Mean	Peak
Radial	1.8	0.0	9.8
Cross track	3.7	0.0	18.4
Along track	6.1	1.1	47.1

Units are millimeters.

nal. During sinusoidal yaw steering the S/C-body roll, pitch, and yaw errors are dominated by a 1 cpr signal, while the SA pitch errors displays a 1 and 3 cpr spectra. A similar spectral analysis over a longer time period indicated that no significant long-term deviations exist.

Figure 3 shows the orbit differences in the radial, cross-track, and along-track components between orbits evaluated using the internal attitude model and the telemetered data. Statistics for this time series are displayed in Table 4. The force model and orbit adjustment parameterization used to compute both these ephemerides is identical to that used in the nominal POE generation. Considering the telemetered attitude as truth, the attitude mismodeling in the radial component of the orbit translates to 1.8-mm level rms errors over the 10-day cycle, with the largest effect (9.8 mm) at the flip, as expected. SLR and DORIS residual analysis indicates that the telemetered attitude orbit is only slightly better than its counterpart and that the effects of the attitude mismodeling in the nominal POEs is negligible. However, the telemetered attitude capability has proven itself to be necessary to accurately process off-nominal attitude events such as the orbital maintenance maneuver 5 (OMM5) between cycles 50 and 51 and OMM6 between cycles 61 and 62.

3.2. Solar Array Temperature Analysis

The current POE T/P thermal model includes a detailed temperature history for the evaluation of the thermal gradient forces on the spacecraft [Marshall and Luthcke, 1994a, b]. Telemetered temperature data from the SA thermal coupons were used to evaluate the SA temperature model and to quantify mismodeling effects within the orbit determination process. Data from the body thermistor coupons were not used, since these instruments are located under the thermal blankets and do not provide the surface temperatures necessary for the thermal model evaluation. Data from four thermistors on the SA front and four from the back, recorded at a 16-s intervals, were used in this analysis. An average temperature for the SA front and back was computed from the four thermistors on each side. These front and back telemetered temperatures were compared to the front and back SA temperatures predicted in the model.

The methodology used for this temperature analysis is similar to that described previously for the attitude analysis. The telemetered SA front and back temperatures were ingested directly into GEODYN and used in the evaluation of the thermal force model computations. These temperatures were also compared with those

Table 5. Solar Array Temperature Differences for Cycle 36
(Internal Model Versus Telemetered Solar Array Temperature)

Statistic	SA Front	SA Back	SA Gradient
Standard	3.07	3.02	2.11
Mean	35.84	34.34	1.49

Units are degrees Kelvin.

predicted by the model. Orbits computed using the internal and telemetered temperatures were also differenced to quantify the effects of SA temperature mismodeling on the orbit quality. The lack of S/C-body telemetered temperatures was a limitation but should not negate the conclusions drawn from this analysis, since the SA has a much larger effect and experiences the greatest temperature fluctuations.

Table 5 shows the statistics for the temperature differences between the internal model and the telemetered temperature over 10 days of cycle 36. The internal model significantly mispredicts the mean temperature of both the front and back of the SA by about 35°K. These large differences are primarily associated with the pitch bias of the SA instituted shortly after launch to protect the S/C batteries that were not considered in performing the prelaunch finite element thermal analysis. However, of more importance is the temperature gradient across the SA, whose modeled mean was found to be within 1.5°K of that measured with a small standard deviation of 2°K over the 10-day cycle. The gradient is the most significant quantity in the computation of the thermal radiation acceleration from the SA. Table 6 displays the statistics for the orbit differences of the internal and telemetered SA temperature orbit cases. The effect of this level of SA temperature mismodeling on the orbit is only submillimeter; there were no significant peaks during either attitude ramp or flip events. Clearly, this analysis indicates that the current macromodeling of SA temperatures is performing at a satisfactory level for precision orbit computations.

3.3. Empirical Accelerations and Macromodel Tuning

When force model errors are much smaller than the forces themselves, as they are for T/P, they can be used in the Hill's linearized equations of motion to relate errors in the spacecraft acceleration to position errors in the orbit. A major portion of the position error is due to resonance effects, caused by the appearance of periodicity or near periodicity in the time series of residual forces, that can be eliminated by adjusting nine parameters in a simple empirical acceleration formula simultaneously with the orbit state [Colombo, 1989; Cretaux et al., 1994]. Because the linearized equations exhibit a critical frequency at zero and at 1 cpr, this formula contains one parameter for the constant and two (sine, cosine) for the 1 cpr acceleration term in each of the three direction components: radial, cross track, and along track. The number of parameters that can be estimated in an actual orbit solution is limited by the strength of the satellite tracking measurement type and distribution and the eccentricity of the orbit. For a circular orbit, radial and along-track accelerations produce inseparable changes to the orbit, and therefore six acceleration parameters suffice.

For relatively small force errors the orbit dynamics acts as a band-pass filter to the highly complex, irregular series of mismodeled forces to produce an orbit position error that is a smooth and simple function of time. It is expected that orbit error, in general, will display a modulated 1 cpr signal, since most of the acceleration

Table 6. Orbit Differences for Cycle 36
(Internal Model Versus Telemetered Solar Array Temperature)

Component	rms	Mean	Peak
Radial	0.2	-0.1	0.4
Cross track	0.2	0.0	0.5
Along track	0.8	0.2	2.9

Units are millimeters.

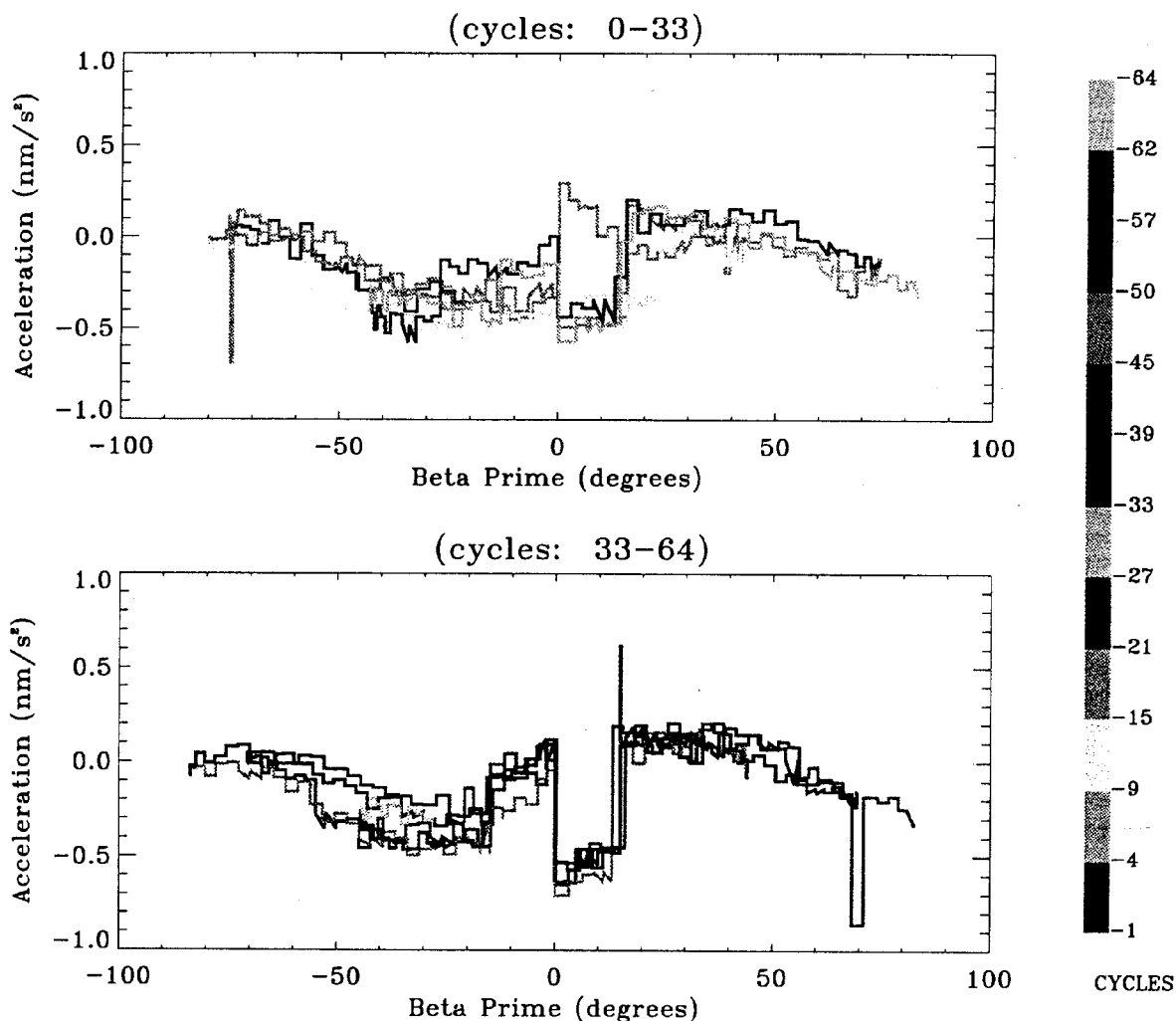


Plate 2a. T/P constant daily along-track empirical accelerations for cycles 1-33 **Plate 2b.** T/P constant daily along-track empirical accelerations for cycles 34-64

error is forced into a 1 cpr position oscillation of constant amplitude in combination with a 1 cpr oscillation having a linear time dependence. For the POE the 10-day orbit solution simultaneously adjusts the orbit state at epoch with the addition of five empirical acceleration parameters per day. These are a constant along-track, 1 cpr (amplitude/phase) along-track, and 1 cpr (amplitude/phase) cross-track acceleration terms and are used to accommodate the neglected forces acting on the satellite to better fit the tracking data. Tailoring the duration over which the averaging takes place and their temporal boundaries allows better accommodation of the orbit error in certain circumstances, such as at the time of the attitude flip maneuver. A bow-tie orbit error effect results from the least squares process that minimizes the error at or near the midpoint spanned by the data. With our adopted POE orbit parameterization a small bow tie is anticipated that will span the 10-day arc, with mini bow ties, spanning each of the 10 single-day segments individually. Coherence across days/arcs is not expected for the series of mini bow ties, as they largely arise from mismodeled nonconservative forces, and these errors depend on highly variable satellite-Earth-Sun geometry.

An evaluation of the history of these recovered empirical accelerations can provide some insight into the character of the modeling inadequacies within the T/P POE. In particular, this section focuses on the performance of the macromodel through different solar aspect regimes and attitude events in which the error characteristics change substantially. Overall, the macromodel accounts for over 95% of the observed accelerations with the residual force accommodated by the adjusted empirical accelerations. Therefore an evaluation of the residual T/P along-track accelerations seen over nearly 2 years of orbit history yields detailed information of the macromodel's performance.

The estimated empirical parameters were analyzed as a function of time and of B' , where B' denotes the angle between the orbit plane and the Sun vector (Marshall *et al.* [1992, Table 4] gives the complete T/P yaw dependence on B'). Each of the acceleration parameter types exhibits very different characteristics with respect to structure and magnitude. The constant along-track accelerations show temporal coherence and a stable signature across B' but represent the smallest signal. The envelope for the magnitudes of these accelerations is from -0.9 to 0.3 nm/s^2 . The 1 cpr accelerations are larger,

Table 7. Adjusted Macromodel Parameter Values

Solution	Specular Reflectivity, Coefficient					Diffuse Reflection, Coefficient	Emissivity, Coefficient		Body Fixed Acceleration, nm/s ²	
	X-	Z+	Z-	SA+	SA-		X-	SA+	X+	Y+
POE	0.295	0.652	0.859	0.139	0.217	1.029	1.066	0.735	0.388	0.201
Global	0.205	0.592	0.632	0.129	0.113	0.941	1.106	0.723	0.296	0.133

POE represents model based on cycles 1 to 15 used to produce precise orbit ephemeris on GDR. Global is 48-cycles solution made for this study.

Table 8. TOPEX/POSEIDON Data Residuals Cycles 1-80

Data Type	Average rms Residual	Average rms Noise	Percent Signal in Residual
SLR, cm	4.4	1.5	67
DORIS, mm/s	0.56	0.53	5

SLR is satellite laser ranging. DORIS is Doppler orbitography and radiopositioning integrated by satellite.

since they are well suited to model residual radiative forces which inherently vary at the orbital frequency. The behavior of the recovered along-track and cross-track 1 cpr accelerations, however, does not exhibit temporal stability for these accelerations are highly correlated within each arc. The magnitude of the along-track 1 cpr accelerations is bounded by ± 3.3 nm/s²; the cross-track 1 cpr accelerations are bounded by ± 15 nm/s² and are poorly constrained by either the tracking data or the physical models. Nonetheless, it is important to adjust these cross-track terms, since significant modeling errors exist in this component and failure to adjust them results in significantly larger residuals and orbit errors.

The constant along-track accelerations display a definitive dependency on β' and a generally symmetric behavior about the flip event (Plates 2a and 2b). After the first three cycles the accelerations are binned by color into six-cycle sets, since it takes approximately 60 days for the satellite to transition across β' between flip events. By doing so, macromodel responses to yaw flip, fix/sinusoidal yaw steering transitions, and full sunlight to occultation regimes become evident. The most prominent feature is the apparent change in the character of the along-track accelerations in the fixed yaw regimes on either side of the attitude flip ($\beta'=0$). At the flip the satellite turns 180° about its Earth-pointing Z axis, such that the X+ and X- plates, whose normal vectors are aligned in the along-track direction during low β' , switch their orientation with respect to the velocity vector. Additionally, there is a change in the along-track projection of the solar array. Therefore the discontinuity at flip represents the directional dependency of the accelerations arising from the X plates, solar array, and applied, constant, body-fixed acceleration in the X₂ direction. This discontinuity is only of the order of 0.2

to 0.4 nm/s² through cycle 33, when the solar array was biased at 57.5°, and increases to 0.6 to 0.7 nm/s² afterward when the solar array was biased at 52.998°. The obvious exception to this behavior occurs during cycle 6, when the solar array was biased in the opposite direction at -57.5°. This strong dependency on SA orientation makes SA warping and SA-with-body interactions candidate sources for this acceleration. Both effects are currently ignored in the macromodel.

Although small, the most unexpected feature in the acceleration history occurs at the full sunlight-to-occultation transition. T/P is in full sunlight when the absolute value of β' exceeds 56°. Observe that for negative β' values there is a distinct change in the acceleration behavior which is dependent on whether the satellite is transitioning into or out of Earth shadowing. Also, when T/P transitions from occultation to full sunlight, there is a larger discontinuity than seen during the opposite transition. This behavior is likely associated with deficiencies in the thermal model. Simplifying assumptions regarding the plate temperatures were made for this transition point [Marshall and Luthcke, 1994a].

The overall magnitude of the accelerations seems to be changing slowly over time, which might indicate physical changes in the S/C surface thermal properties or in the magnitude of the anomalous acceleration itself. The macromodel used in producing the POEs was tuned using the first 15 cycles of SLR and DORIS tracking data. To accommodate the observed anomalous force, a set of

Table 10. Regional Summary of Guier [1965] Analysis of SLR Residuals From GPS Orbits

Region	Mean Bias (cm)
North America	0.9
Europe	3.0
Pacific	-0.3
South America	0.9
Australia	0.6
Asia	4.5

Table 9. Precise Orbit Ephemeris Versus Global Positioning System Orbit Differences, Cycles 10-50

	TOD Radial	TOD Cross-track	TOD Along-track	TOD X	TOD Y	GRF X	GRF Y	Z
Mean	-0.33	-0.43	-3.13	-0.12	-0.30	2.02	1.01	2.89
Standard deviation	3.36	7.59	10.83	8.31	8.06	8.34	7.71	7.35

TOD is inertial true of date system. GRF is Greenwich reference fixed system. Units are centimeters. Cycles 26-29 have been omitted for all but the radial statistics because of GPS timing biases.

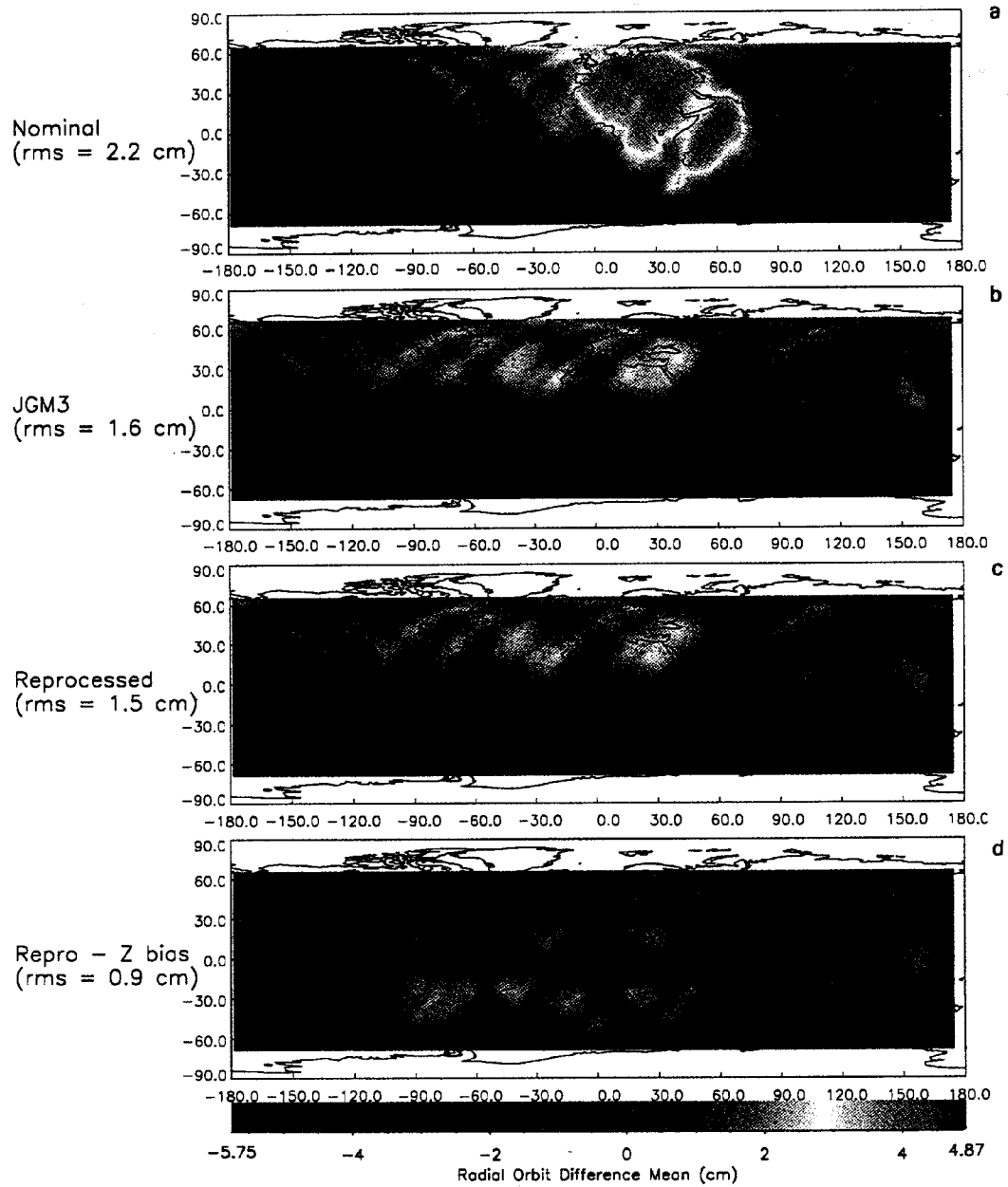


Plate 3. Mean of radial orbit differences between Precise Orbit Ephemeris (POE) and Global Positioning System (GPS) T/P ephemerides. (a) Nominal POE versus GPS. (b) JGM-3 POE versus GPS. (c) Combined POE (improved gravity, tide, and nonconservative force models) versus GPS. (d) Z bias removed, POE versus GPS.

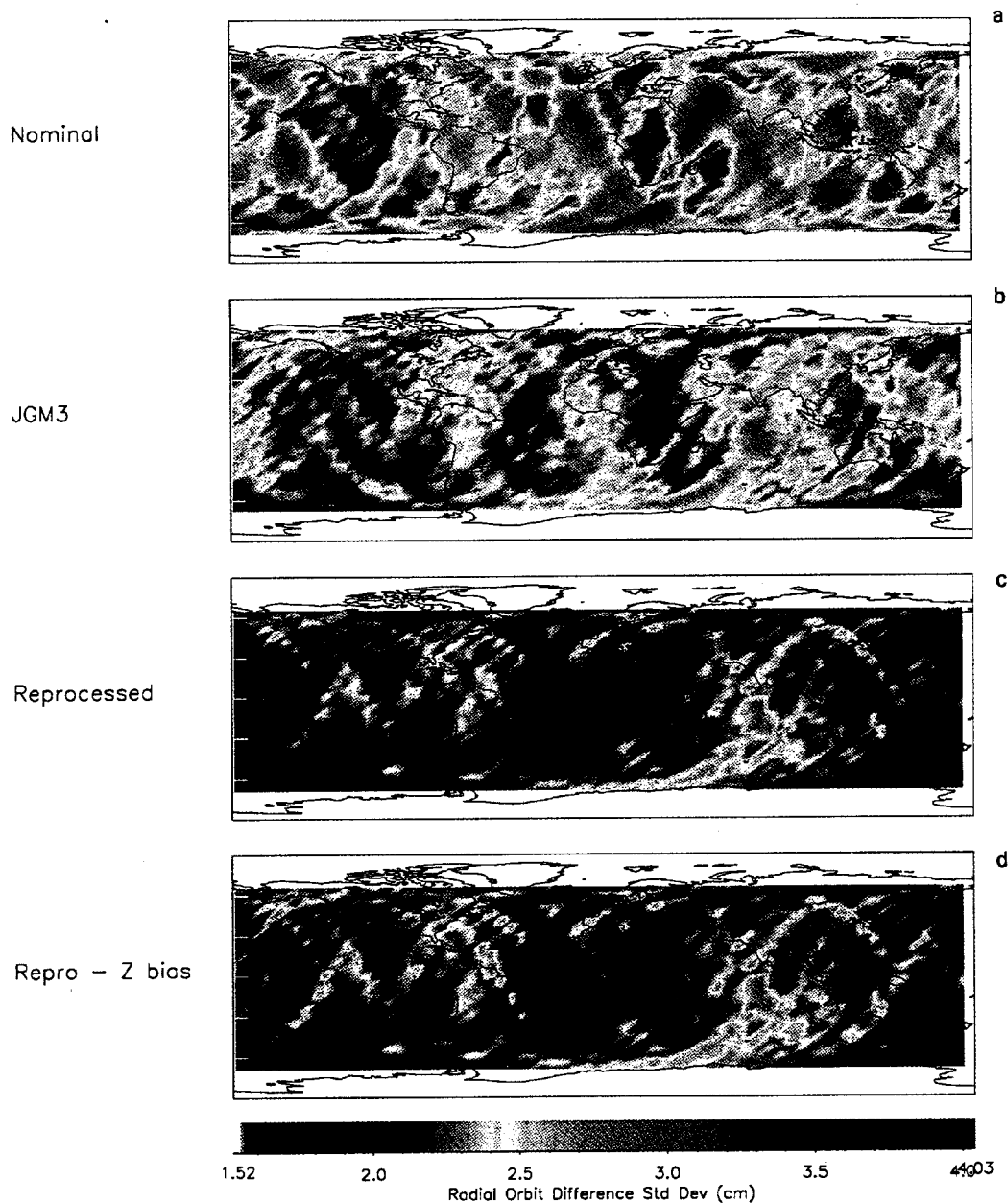


Plate 4. Standard deviation of radial orbit differences between POE and GPS T/P ephemerides. (a) POE versus GPS. (b) Standard Deviation of JGM-3 POE versus GPS. (c) Standard Deviation of Combined POE versus GPS. (d) Standard Deviation of Z bias removed, POE versus GPS.

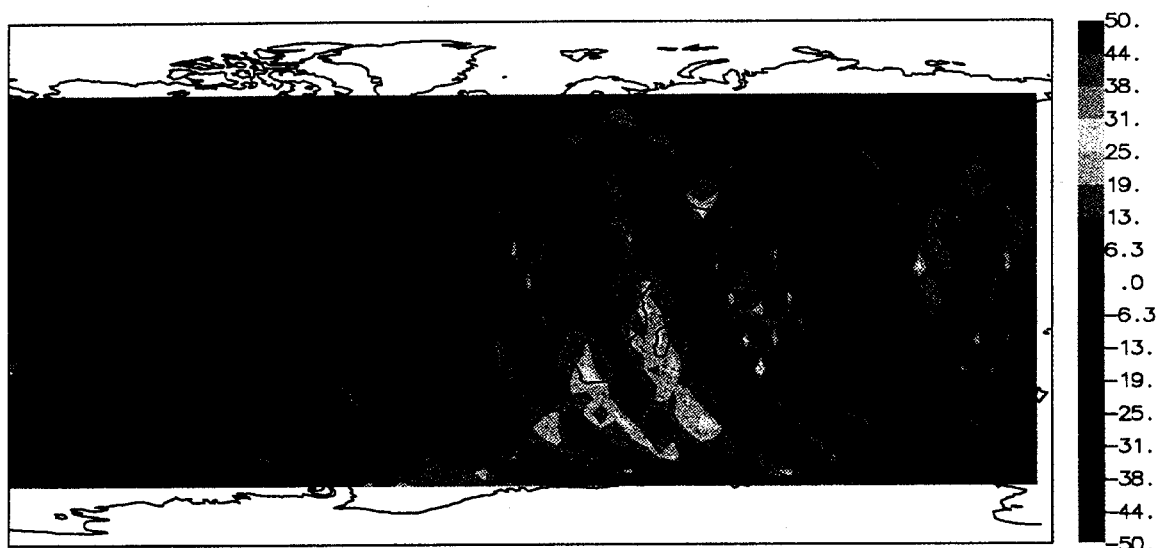


Plate 5. Mean radial orbit differences between POE and GPS T/P ephemerides (collinearly differenced with respect to cycle 15).

body-fixed X and Y accelerations were estimated as well [Marshall and Luthcke, 1994b]. Material property degradation and/or changes in the characteristics of the anomalous force are not accommodated in this process, and therefore the nonconservative force modeling error could increase with time. This hypothesis is examined through a "retuning" of the macromodel.

Four sets of body-fixed accelerations and macromodel parameters were independently adjusted for cycles 1 through 48. Each set of 12 cycles span one complete period of the B' oscillation to assure a full sampling geometry. Recovered parameter values from the four sampled periods do not reveal degradation in the material properties of the body, but those of the solar array do seem to reflect likely physical degradation. There is evidence that anomalous forces on the satellite in earlier cycles have decreased and that TOPEX/POSEIDON has now reached a steady state with respect to nonconservative forces.

Additionally, one set of parameters was adjusted over all 48 cycles and termed the "global" macromodel. Table 7 compares the recovered parameter values from the original POE and new global macromodels. The global model, which incorporates the "quieter," latter cycles, better represents the steady state behavior of the macromodel and would better accommodate later cycles. We see no evidence with the implementation based on this analysis approach that the orbit modeling accuracy is degrading in time because of changes in the physical characteristics of T/P while on orbit. Overall, it is important to keep sight of the fact that the estimated acceleration parameters effectively account for the described deficiencies in the macromodel that might otherwise affect the orbit accuracy.

4. Measurement Modeling

The SLR and DORIS measurements are very precise. SLR measures the time it takes for an optical pulse to traverse the distance from observer to satellite and back. DORIS is a one-way integrated Doppler, measuring the range difference between selected observation times; we divide by the time interval between successive obser-

vations in each pass to construct one-way average range rates. Both measurement types fundamentally are based on precise ranging, and therefore the formulation for these measurements is based on the range modeling. The range is computed from the Cartesian positions of the spacecraft and observer, taking into account the travel time of the signal in vacuum (speed of light). Corrections are made for path delay/refraction effects and for the geometric distance of the instruments phase centers with respect to the center of mass of the S/C.

For SLR the refraction errors are small, since optical wavelengths exhibit well-understood behavior when traversing the atmosphere using the adopted Marini-Murray model. For elevation angles above 20° , these corrections are accurate to ± 5 mm. In addition, the T/P laser retroreflector array provides a very different target than the ideal specularly reflecting sphere. The target response is the sum of the individual corner cube responses; they form a complex and elongated pulse train in the time domain. The received waveform at the detector electronics is no longer a simple slightly distorted Gaussian pulse. The far-field diffraction pattern (FFDP) computations require additional convolutions. The response of the receiver electronics to this more complex signal requires modeling; for the T/P project, over 20 different receiver models had to be developed to model the laser range correction to the subcentimeter level [J. J. Degnan, personal communication, 1993].

With DORIS, the ionospheric propagation delay estimation based on the 2-GHz and 400-MHz dual-frequency signals is highly accurate and eliminates this effect well within the noise level of the DORIS system, except for instances of extremely high solar activity. The adopted troposphere model for DORIS is a modified Hopfield model using the observed pressure, temperature, and humidity. However, its performance is degraded, principally due to the wet component. We estimate a tropospheric refraction scale bias for each pass in order to detrend the data for this measurement modeling error. A constant bias per pass is also adjusted for the DORIS data to eliminate the unknown frequency offset between the station transmitter and the T/P receiver.

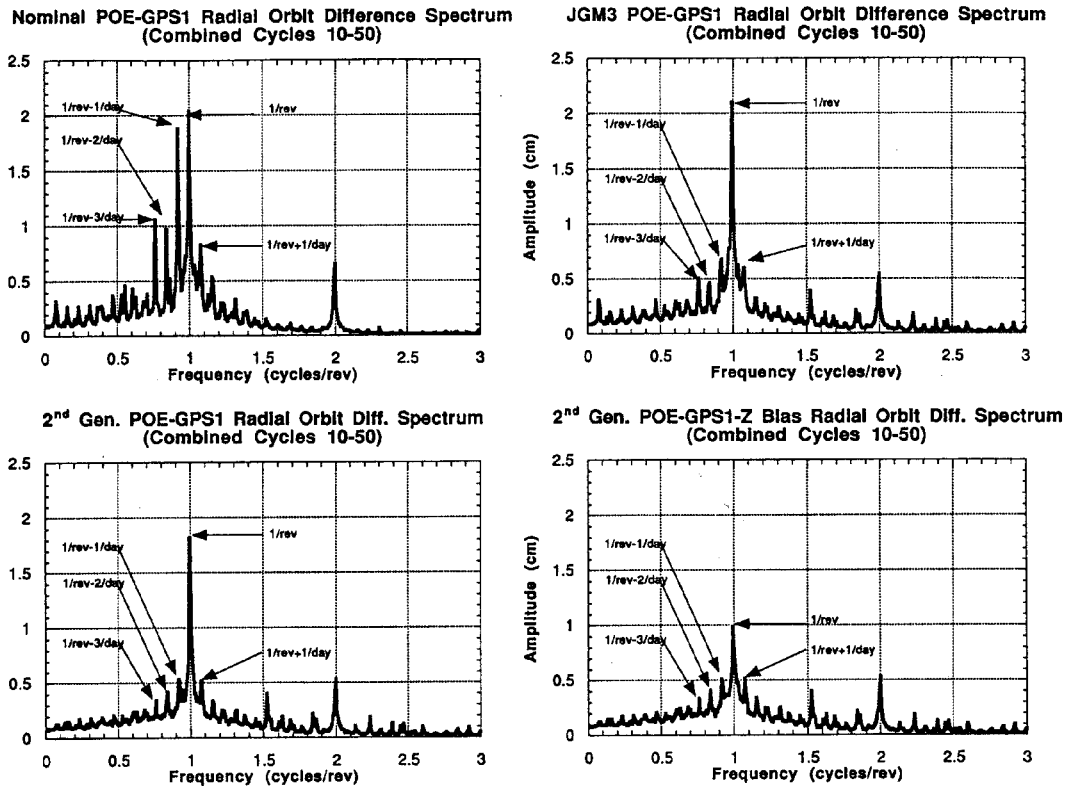


Figure 4. Combined amplitude spectrum of POE versus GPS radial orbit differences. (a) Nominal POE versus GPS. (b) JGM-3 POE versus GPS. (c) Combined POE (improved gravity, tide, and nonconservative force models) versus GPS. (d) Z bias removed POE versus GPS.

In summary, both data types are state of the art for ranging and Doppler tracking systems, and measurement modeling for the SLR and DORIS data is quite advanced. The performance of these systems, as derived from the orbit solutions on T/P, is described in Table 8. A noise level estimate of the data is obtained by removing a measurement and timing bias from each pass of residuals. The remaining postfit rms reflects the data noise level, since the estimated biases remove the vast majority of the tracking systematics and orbit error. As shown in Table 8, considerable signal remains in the SLR residuals, whereas the DORIS residuals are close to the noise floor. This suggests a higher relative weight should be applied to the SLR data in the orbit solution. These data and their misfit within orbit solutions can provide additional insight into the temporal and spatial character of orbit error. As described below, this approach has been used to provide a somewhat external means to assess the behavior of POE error.

5. Observed Temporal And Spatial Orbit Error Characteristics

As stated previously, no single test can completely quantify the orbit error in the POEs. Consequently, one must rely on a battery of tests, each evaluating a particular aspect of orbit error. Operationally, each POE is evaluated based on over 200 criteria as a quality control measure [Putney *et al.*, 1993]. In aggregate, all these tests confirm that the POEs are radially accurate to within 3-4 cm rms for any 10-day cycle. The focus of this paper is a characterization of this remaining orbit error. This assessment heavily relies on a com-

prehensive comparison of the SLR/DORIS determined POE orbits and their GPS reduced dynamic counterparts.

5.1. Overview of Orbit Determination Methodologies

The GPS reduced dynamic orbit and SLR/DORIS dynamic solutions share neither data nor equal dependence on force modeling. Therefore a comparison of ephemerides computed from these methods can effectively isolate the unique error characteristics of each. The methods themselves are briefly reviewed below.

Bertiger *et al.* [1994] and Yunck *et al.* [1994] describe in detail the methodology used to compute the T/P orbits using GPS tracking

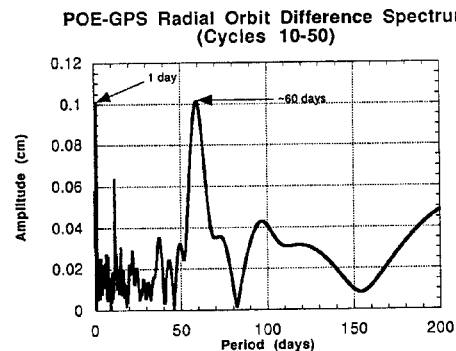


Figure 5. Amplitude spectrum of POE versus GPS radial orbit differences (cycles 10-50).

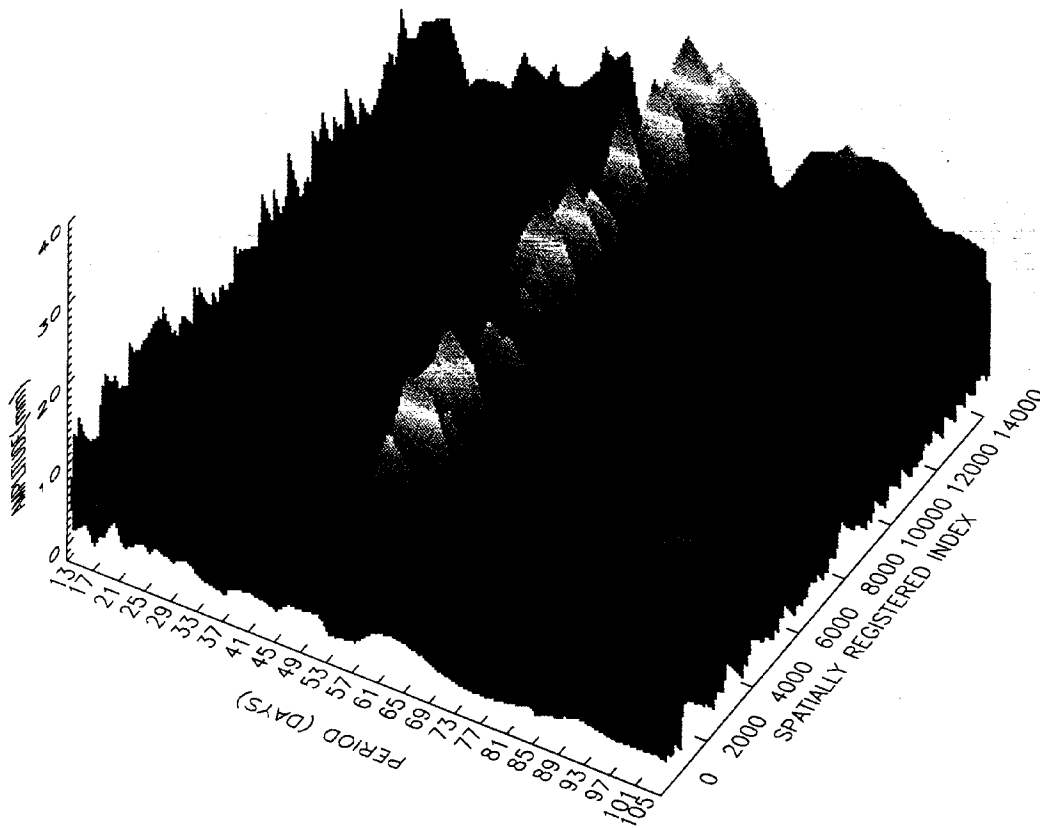


Plate 6. Amplitude spectrum of POE versus GPS radial orbit differences at fixed geographic points.

and a reduced dynamic methodology. This technique uses a stochastic sequential filter to reduce the GPS observation residuals obtained from an a priori dynamically determined solution. Thirty-hour arcs are used, each overlapping the following by 6 hours. The segments are spliced together using a cosine taper smoothing to obtain a continuous 10-day arc. In addition to a host of other parameters, stochastic accelerations are determined every 5 min with a 15-min process noise correlation time. A balance is achieved in the weighting of the GPS information with respect to the dynamic trajectory for optimal orbit accuracy (with the weighting extremes representing either a purely geometric three-dimensional (3-D) GPS navigated orbit versus the original dynamic orbit). This approach significantly reduces the dynamic modeling error but, at the same time, is more susceptible to measurement and reference frame errors.

Nerem et al. [1993], *Putney et al.* [1993], and *Tapley et al.* [1994a] summarize the fully dynamic, least squares, batch process used to compute the POEs from SLR and DORIS tracking data. Single solutions for each 10-day cycle are computed, estimating the T/P state and daily along-track and cross-track empirical accelerations. This orbit determination approach depends on the equations of motion and exhibits errors, which are overwhelmingly a function of force mismodeling.

The actual orbits available also differ because of modeling details. The Earth orientation parameters (EOP) and the reference frames employed by each center (Jet Propulsion Laboratory [JPL] for the GPS orbits, Goddard Space Flight Center for the

SLR/DORIS orbits) can also introduce significant orbit differences [Rosborough, 1993]. For the GPS orbits, EOP parameters were estimated from the GPS data, whereas in the POE solutions, EOP values were obtained from solutions based on LAGEOS SLR data. These SLR EOP values are in the standard International Earth Rotation Service (IERS) reference system. Orbit comparisons can therefore yield differing results, depending on the reference system (i.e., inertial or Earth fixed) used in the comparison. The following three geocentric coordinate systems are applicable when comparing these orbits: (1) the inertial true of date (TOD) is a right-handed system, which has the X axis pointing to the true vernal equinox and the Z axis aligned with the Earth's instantaneous spin vector; (2) the pseudo Earth fixed or Greenwich reference fixed (GRF) differs from the TOD by only a rotation about the Z axis through the Greenwich apparent sidereal time (GAST) angle, so that the X axis is directed along the meridian of Greenwich and the system rotates with the Earth; (3) the crust-fixed terrestrial reference frame (TRF) differs from the GRF system by a rotation given by the polar motion angles, so that the Z axis coincides with the IERS defined mean pole.

To achieve a comparison free of EOP introduced differences in the TOD comparisons, the GPS orbit was rotated into a reference frame more consistent with the POE TRF in order to eliminate the direct effect of the EOP differences. This was accomplished by rotating the GRF position of the GPS orbit to the TOD system using the GAST angle on the GSFC POE. It would have been more consistent in terms of the spin axis to rotate the GPS TRF position to

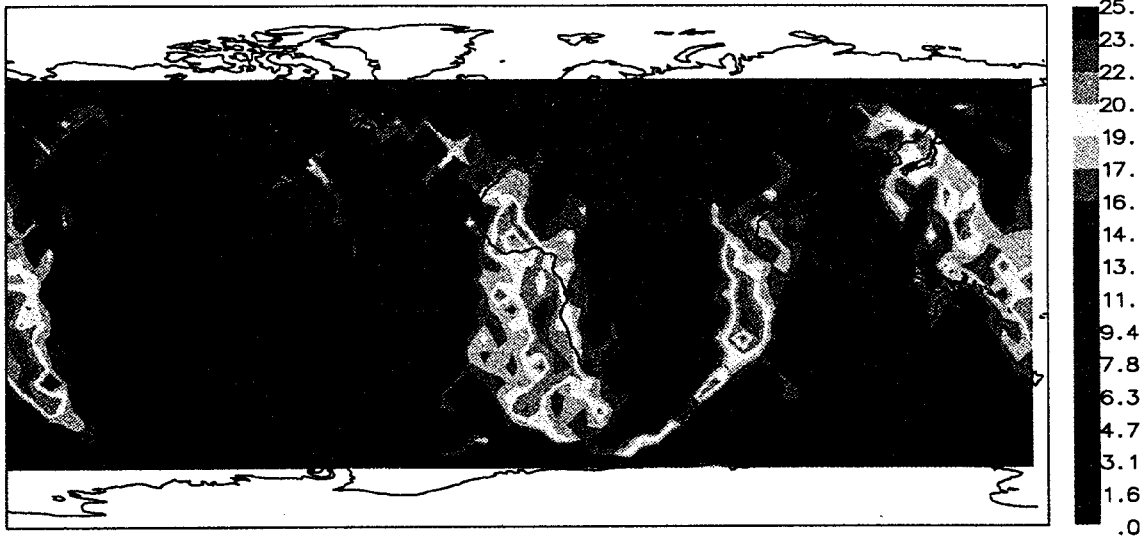


Plate 7a. Geographic distribution of 61-day period amplitudes from Plate 6.

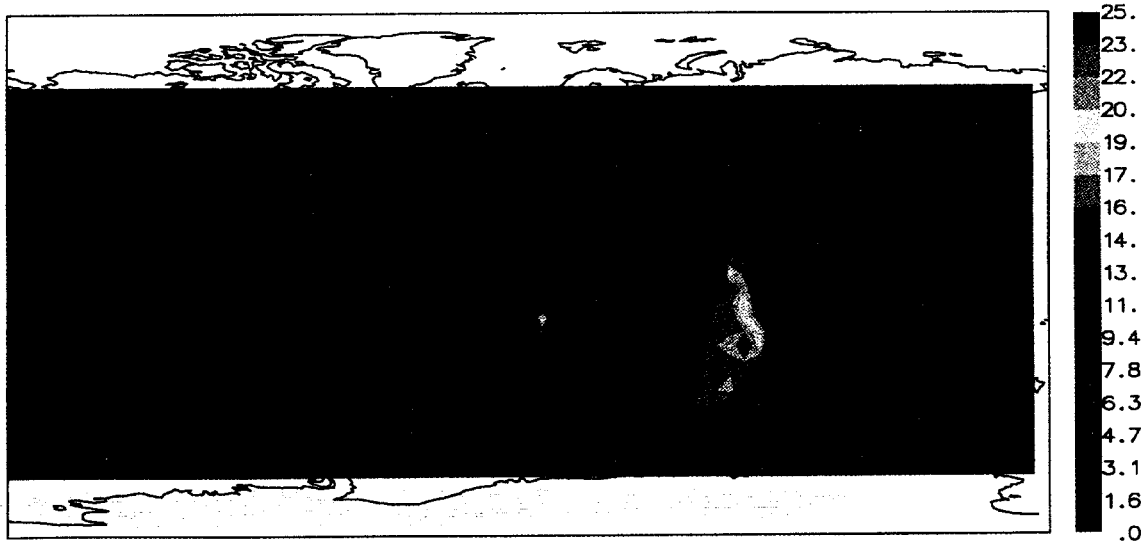


Plate 7b. Geographic distribution of 61-day period amplitudes of POE, with improved ocean tide model, versus GPS radial orbit differences at fixed geographic points.

Table 11. Comparison of Statistics for Orbits Produced Using Different Gravity Models

	JGM-2	JGM-3
SLR residuals	4.03	3.84
POE versus GPS radial orbit differences	3.38	2.82
POE versus GPS geographically correlated radial orbit differences ^a	2.22	1.57

Units are rms centimeters.

^a Mean ascending and descending passes over a 5x5° block were used.

Table 12. Comparison of Statistics for Orbits Using Different Ocean Tide Models, Cycles 10-50

	Nominal	Improved
SLR residuals	4.03	3.75
POE versus GPS radial orbit differences	3.38	3.27
POE versus GPS geographically correlated radial orbit differences ^a	2.22	2.24

Units are rms centimeters.

^a Mean ascending and descending passes over a 5x5° block were used.

TOD using the GSFC values for polar motion and GAST. *Rosborough* [1993] has demonstrated that the orbits compare better starting with the GRF system. A discussion and quantification of these orbit intercomparisons follows.

5.2. Radial Orbit Comparison Methodology

Portions of 37 cycles (10 through 50) were used for this comparison. The POE and GPS values of T/P radial position were compared at 1-min intervals. The GPS orbits did not always span a full 10-day cycle, and it was also necessary to eliminate large differences at the beginning and end of the cycle, where the GPS orbits occasionally experience edge effects associated with their filtering scheme. Only an integral number of revolutions of overlapping data were compared for each cycle, beginning and ending with an equator crossing. Table 9 presents summary statistics for comparisons in each coordinate system.

Spectral Analysis of POE-GPS Radial Orbit Differences in the Spatial Domain (Geographic RMS) (Cycles 10-50)

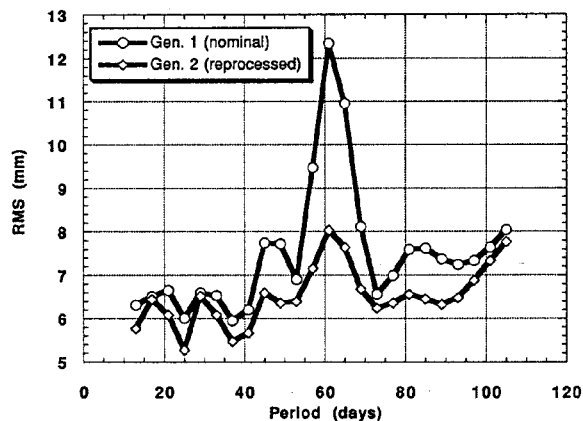


Figure 6. Geographic average rms amplitude spectrum of POE versus GPS radial orbit differences (nominal versus improved ocean tide model).

5.3. Temporally Invariant Orbit Differences

As discussed earlier, certain force modeling errors result in geographically correlated orbit error. Given that the GPS reduced dynamic method is less sensitive to these errors, geographically correlated error is revealed in the resulting orbit differences [Christensen et al., 1994]. However, differences in the definition of the terrestrial reference frame also exhibit time-invariant characteristics. Realization of a TRF is both complex and approximate. While great progress has been made in the unification of an International Terrestrial Reference Frame (ITRF) [cf. Boucher and Altamimi, 1991], all individual solutions deviate from this established system at the few centimeter level. When orbit differences are investigated at the few centimeter level, as for T/P, the discrepancies in the reference frame definition, especially across tracking technologies, have to be assessed.

In order to gauge the time-invariant component of the radial orbit difference, the full time series was spatially registered. A database was formed in which the radial orbit differences from each 10-day repeat cycle were stored for each geographic point with values interpolated to registered locations based on the cycle 18 ground track. Statistics were computed across all cycles at each grid point. Plates 3a and 4a display the geographic distribution of the mean and standard deviation about this mean of the radial orbit differences. The dominant feature seen in Plate 3a is quite similar to the geographically correlated error predicted from the JGM-2 error covariance (Plate 1). The mean orbit differences exhibit a large systematic offset over Europe and the South Pacific at the magnitude predicted by the JGM-2 covariance.

To assess reference frame consistency, the reduced dynamic GPS ephemerides were imported directly into the GEODYN orbit determination system used to compute the POEs [Rowlands et al., 1994] and SLR residuals were computed. Lasers provide the most accurate and least ambiguous measurements for orbit positioning on an observation-by-observation basis and are strong contributors to the adopted ITRF. The SLR site locations used were those adopted for the POE, which were obtained from SLR tracking of the LAGEOS satellite by the Center for Space Research, University of Texas. These station coordinates are completely compatible with our adopted polar motion series which originates from the same source.

Table 13. Comparison of Statistics for Orbits Using Different Nonconservative Models, Cycles 10-50

	Nominal	Improved
SLR residuals	4.03	3.98
POE versus GPS Radial Orbit Differences	3.38	3.36
POE versus GPS geographically correlated radial orbit differences ^a	2.22	2.21

Units are rms centimeters.

^a Mean ascending and descending passes over a 5x5° block were used.

Table 14. Orbit Statistics Using Alternative Data Weights and Empirical Parameterization, Cycles 43-48

	Nominal	New Weight	8-Hour C_d	Combined
SLR residuals	3.8	3.6	3.2	3.0
DORIS residuals	0.57	0.57	0.56	0.56
POE versus GPS radial orbit differences	3.0	3.1	2.8	2.6
POE versus GPS Along-track orbit differences	11.7	12.0	10.0	9.5

Units are rms centimeters. C_d is drag coefficient.

Table 15. Orbit Statistics Using Combined Model Improvements, Cycles 10-50

	Generation 1	Generation 2	Z Bias Removed
SLR residuals	4.03	2.46	
POE versus GPS radial orbit differences	3.38	2.44	2.13
POE versus GPS geographically correlated radial orbit differences ^a	2.22	1.45	0.94

Units are rms centimeters.

^a Mean ascending and descending passes over a 5x5° block were used.

An evaluation of the resulting SLR observation residuals provides insight into reference frame differences based on the absolute ranging quality of each SLR measurement. Using the *Guier* [1965] approach, the radial, across- and along-track orbit errors were estimated for each pass of SLR residuals. Table 10 shows a region-by-region estimate of this bias. A significant part of the mean difference between GPS and SLR/DORIS orbits in the Earth-fixed X and Y directions must arise from differences in the adopted TRF in the GPS and SLR/DORIS computations.

5.4. Collinear Orbit Differences

Any geographically correlated, time-invariant signal can be removed by taking collinear differences with respect to a selected cycle at each spatially registered point. This collinear differencing leaves, as its residual, the time-varying signal arising from sources, such as tidal and nonconservative force modeling errors, and completely eliminates all errors arising from the static geopotential field when applied to the frozen T/P orbit. Cycle 15 was selected as the reference, since T/P was in full sunlight throughout this cycle, thus eliminating thermal transitions as a potential error source in the nonconservative force modeling. Plate 5 displays the geographic distribution of the mean POE-GPS orbit differences (cycles 10-50) after the POE-GPS difference for cycle 15 was removed from all the other cycles at each geographic data point. Plate 5 demonstrates that the long wavelength spatially coherent pattern is nearly eliminated.

This collinear differencing technique also reveals information on the nonconservative force model error. When the reduction of the radial difference as a function of the average β' value for each cycle in the collinear differencing is examined, it becomes clear that cycles with high (absolute) β' values, similar to cycle 15, have sim-

ilar nonconservative force model error signatures and exhibit the most reduction in orbit differences through the collinear differencing process. Likewise, cycles having β' values near zero and that are maximally occulted show the least reduction in signal after collinear differencing with cycle 15. Clearly, even with the empirical accelerations, small nonconservative force model errors remain in the POEs and exhibit a periodic behavior. For cycles with the same β' as the reference cycle, this error source is removed in the collinear difference.

5.5. Spectral Analysis of Orbit Differences in the Temporal Domain

The radial orbit difference time series was spectrally analyzed for periodic signal within each 10-day repeat cycle and over the entire 410-day span. Least squares spectral analysis was used to process both the evenly spaced and unevenly spaced time series [cf. *Wells and Vanicek*, 1978]. Complex demodulation (cf. *Francis and Berge*, 1993) was also used to extract any long-period term modulating the 1 cpr over the 410-day span. The rms combined amplitude spectra of the orbit differences over cycles 10-50, shown in Figure 4a, has the majority of the power in the 1 cpr, followed by 1 cpr modulated by 1, 2, and 3 cpd terms. These frequencies account for over 50% of the variance. Little variation in the spectra between the 10-day cycles was observed. A 1 cpr frequency is generally expected and stems from a combination of a number of sources including geographically correlated orbit error, nonconservative modeling errors in the POE, and/or reference frame offsets. Equations (1) and (2) indicate that modulation of the 1 cpr likely results from errors in the $m=1, 2, 3$ m -daily gravity perturbations although offsets in the TRF are also source candidates. A small 2 cpr term was also present, which is an artifact of the estimation of a 2 cpr acceleration param-

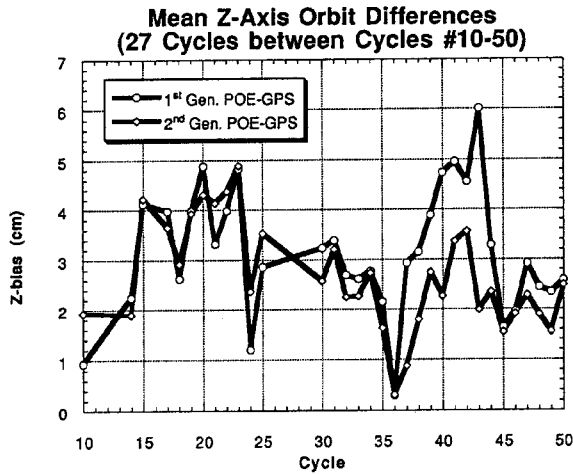


Figure 7. Average Z bias between the POE and GPS over cycles 10-50.

eter in the GPS dynamic solution which is not done in the SLR/DORIS POE solutions. Tests indicate that this signal is unlikely to be caused by force model deficiency and suggest that the 2 cpr acceleration parameter should not be estimated.

The frequency spectrum for the full 410-day time series displays no significant long-period signal (Figure 5). The maximum power appears at periods around 1 and 60 days but is submillimeter in amplitude. This broadband 60-day peak is consistent with half the synodic period of the T/P orbit B' and could be indicative of a time dependency in the nonconservative force model error in the POEs being a function of B' . This result is consistent with the level of error found when testing telemetered versus modeled S/C attitude and thermal behavior.

5.6. Spectral Analysis of Orbit Differences in the Spatial Domain

Previous analysis has shown no significant long-term trends exist in the orbit difference time series spectra. However, when discussing the characteristics of orbit error, it is important to consider the impact of the orbit error on oceanographic analyses. In particular, one must consider how the orbit error changes temporally at a fixed geographic location. This is accomplished through a spectral analysis of the orbit difference time series at each of the 14,400 latitude/longitude grid points in our orbit difference database. Plate 6 presents a three-dimensional map of the power spectra of these geographically dependent effects. A majority of the strong signal lies at a 61-day period, with up to 2- to 3.5-cm amplitude peaks. The 61-day period has a 1.4-cm global rms, accounting for approximately 40% of the total variance. A 45-day period is the second most powerful term, with a global rms amplitude of 0.9 cm. The geographical

distribution of the amplitudes for the 61-day period at the grid points reveals maximum effects in the Indian Ocean, the southeastern Atlantic off the coast of Africa, and the Pacific Basin (Plate 7a). Note that all the maxima lie over ocean regions. An evaluation for the source of these orbit errors follows.

5.7. Improved Gravity Field Modeling

To quantify the effect of gravity modeling error on the geographically correlated orbit error, all the cycles of SLR/DORIS data were reprocessed using the JGM-3 gravity model [Tapley *et al.*, 1994b] and compared to the nominal POEs and the GPS orbits. This geopotential field directly incorporates GPS tracking data taken on T/P into the JGM-1 model. The strength of the GPS data improves the geopotential model, especially for the $m=1$ terms, as is seen in the significant reduction of the geographically correlated error arising from these terms when the JGM-3 error covariance is projected onto the T/P orbit. Covariance projections indicate that the geographically correlated radial error for JGM-3 is 0.6 cm rms, as compared to the 1.6 cm predicted for JGM-2. Results are summarized in Table 11. With the inclusion of JGM-3 the radial orbit differences were reduced by 1.9 cm and the geographically correlated orbit error dropped by 1.6 cm. This is consistent with the JGM-2 covariance prediction that the gravity field contributes approximately 1.6 cm rms to the geographically correlated orbit error. Plates 3b and 4b shows the resultant geographically correlated orbit error. The high over Europe and the low in the South Pacific are eliminated, and the picture is dominated by a northern hemisphere high-southern hemisphere low signal. This is consistent with a Z-axis coordinate bias between the POE and GPS orbits and will be discussed in more detail in section 5.11.

With the use of JGM-3 the frequency spectrum of the orbit differences with respect to the reduced dynamic orbits is considerably simplified (Figure 4b). As before, the spectrum is dominated by the 1 cpr term. However, the powers at 1 cpr modulated by 1, 2, and 3 cpd have dropped markedly to approximately 0.5 cm. The power spectra of the SLR/DORIS orbit differences (JGM-2 versus JGM-3) find power residing in the 1 cpr and the 1, 2, 3 cpd modulating terms. This is consistent with known changes in the $m=1, 2, 3$ gravity coefficients (as described by Tapley *et al.* [1994b]), which give rise to changes in the m -daily orbit perturbations. Also note that Figure 4b also exhibits a spike at 1.5 cpr that did not appear in Figure 4a. Tests demonstrate that this is a result of the difference in the JGM-3 gravity field model used in the SLR/DORIS orbit and the JGM-2 model used in the GPS dynamic orbit and reflects the reduced dynamic technique's dependency on the a priori force models.

5.8. Improved Background Tidal Modeling

We tested the hypothesis that at a given geographical location, T/P radial orbit errors having a near 60-day period are because of regional S_2 and M_2 tide errors in the background model. Bettadpur and Eanes [1994] have developed an analytical formulation which

Table 16. First- and Second-Generation POE-GPS Orbit Differences (for 27 Cycles Between Cycles 10 and 50)

	Radial rms	Cross-Track rms	Along-Track rms	Z Bias Mean
POE G1-GPS G1	3.34	7.54	11.29	2.87
POE G2-GPS G1	2.42	5.11	6.83	2.82
POE G2-GPS G2	2.27	4.50	6.12	2.63

G is generation. Only 27 second-generation GPS trajectories are currently available. Units are centimeters.

Table 17. POE Parameterization Characteristics

Model	Nominal POE	Second-Generation POE
Gravity field	JGM-2	JGM-3
Ocean tides	<i>Schwiderski</i> [1983], 6000 terms	<i>Ray et al.</i> [1994], 35,000 terms, 15x15 +
Nonconservative forces	GSFC macromodel, cycles 1-15	GSFC macromodel, cycles 1-48
Empirical parameters	1 rpd along track	1 rpd along track
	1 rpd cross track	1 rpd cross track
	1 per day constant along track	1 per 8-hour drag
Data weighting	nominal	upweight SLR 2x
Station coordinate and EOP	CSR93L02/CSR94L01	CSR95L01
Secular pole rate	Pavlis (LAGEOS)	Gross (Space 1993)

Abbreviations are as follows: GSFC, Goddard Space Flight Center; rpd, revolution per day; SLR, satellite laser ranging; and CSR, Center for Space Research.

relates the errors in the ocean tide models to corresponding satellite orbit errors. Their work corroborates this hypothesis. The largest tides on the ocean surface arise from the solar and lunar semidiurnal tides, S_2 and M_2 constituents; in the diurnal band, O_1 and K_1 are dominant. These four tides account for more than 95% of the ocean tidal variance on the Earth's surface. The aliasing (or sampling) periods for these tides by the T/P orbit ground track are shown in Table 2, with the M_2 , S_2 , and O_1 aliasing periods matching closely the near 60- and 45-day peaks seen in the power spectra of the spatially registered orbit differences.

As discussed in section 2, the background tide models used for POE orbit computations are based on the *Schwiderski*, [1983] tide models and designed to tolerate centimeter-level radial omission errors. The shortcoming in this *Schwiderski*-based background model, dominated by M_2 , S_2 , and O_1 errors [cf. *Schrama and Ray*, 1994], is believed responsible for the 60- and 45-day periodicities seen in the orbit differences at various geographic locations. To confirm this hypothesis, tests were run to quantify the magnitude of the omission and commission error in the background tidal model.

Omission error refers to the mismodeling that results from the exclusion of terms in the tide model. In order to gauge the magnitude of the effect of the omitted terms, prograde and retrograde background tidal models complete to degree and order 15 were used for orbit computations. These tests were previously reviewed by *Nerem et al.* [1993] and showed 0.8-cm global rms radial errors on T/P due to omitted tidal terms in the background model. The excellent orbit accuracy achieved on T/P has allowed significant advancement in global ocean tidal modeling. Many investigators have developed corrections to the standard *Schwiderski* models that significantly reduce commission errors associated with the diurnal and semidiurnal bands. We adopted the new T/P-based tide models developed by *Ray et al.* [1994]. Therefore the background tide model used for these orbit computations was composed of the dynamically derived long-wavelength terms adjusted from tracking data, with the remainder of the model coming from the *Ray et al.* [1994] model. The *Schwiderski* models, also complete to 15 x 15, were used for the longer-period M_m , M_f , and S_{sa} bands.

A complete set of T/P orbits were computed using this new tide model. Computation times were dramatically increased, given this model now required evaluation of more than 35,000 tidal harmonic terms. These new orbits were compared to the GPS reduced dynamic orbits and the spatially registered database restructured. Table 12 presents a comparison of the orbit results using the original and new tide models. Clear improvement is seen with the more correct and complete T/P-based tide model. Although the characteristics of the geographic distribution of the time-invariant orbit dif-

ferences and the corresponding amplitude spectrum of the orbit difference time series remain largely unchanged from the nominal POE, the enhanced tidal model greatly reduces the amplitudes observed in the spatial component of the spectrally analyzed differences. Figure 6 presents the geographically averaged power spectra based on these new comparisons and shows the global rms of the 61-day period dropping to approximately 1.0 cm. Plate 7b displays the corresponding geographic distribution of the 61-day signal. Note that the high amplitudes associated with the southern oceans have largely been removed. These results confirm that background tidal modeling limitations are significant contributors to the error in the NASA POE. Furthermore, since the POEs have geographically dependent orbit errors having the tidal aliasing periods, it is likely that the T/P-based tide models are corrupted to some extent. An iteration of these tidal solutions is therefore warranted using orbits based on this new tide model.

5.9. Improved Nonconservative Force Modeling

All cycles were processed with the new macromodel tuned with data from cycles 1-48. Fits to the data, radial differences with the POE, and recovered parameterization were analyzed. Table 13 shows the statistics for the analyzed cycles. The results show a significant improvement in the laser fits for cycles, which include attitude events and little improvement for quiet cycles when using the global macromodel. Overall, a modest improvement in the fits is observed. Spatial and temporal differences with the GPS orbits remain largely unchanged. The magnitude of the recovered along-track constant accelerations demonstrate that, as expected, the POE macromodel performs better than the global version over the early cycles. However, the global model yields smaller residual accelerations for the later cycles. Furthermore, the values tend to be more smooth around attitude events ($\theta \sim 0$) where the modeling is most deficient.

Table 18. Spatial and Temporal Radial rms Orbit Error Characteristics

	Nominal POE	Second-Generation POE
Geographically correlated	1.9	0.9
1 revolution	2.1	1.0
1 revolution modulated by 1, 2, 3 cpd	1.5	<0.4
Daily term	0.6	0.3
Dynamic tide error, (61-day period)	1.0	0.7

Units are rms centimeters.

Table 19. T/P Radial Orbit Error Budget

	Mission Specifications	Nominal POE	Second-Generation POE
Gravity	10	2	1
Solar radiation pressure	6	2	2
Atmospheric drag	3	1	<1
GM	2	1	1
Earth and ocean tides	3	1	1
Troposphere	1	<1	<1
Station location	2	1	1
Total radial orbit error	12.8	3.5	<3

Units are rms centimeters. GM is the universal gravitational constant times the mass of the Earth.

5.10. Alternative Data Weighting and Empirical Parameterization

As discussed in section 4, an investigation into the relative contributions of the SLR and DORIS data revealed that significant signal remained in the SLR data, whereas the DORIS data fit was only slightly above the system noise floor. Therefore, after a careful review of the SLR biases, the relative weight of the SLR data with respect to DORIS was increased by a factor of 2 to strengthen the effect of SLR in the orbit solution.

Also, a prominent daily along-track signal is observed in the orbit differences. This signal remains strong, even when the improved gravity, tide, and nonconservative force models are used for the POE. Adjustment of gravity terms in the SLR/DORIS solution diminish these along-track differences and indicate further refinement of the conservative and nonconservative force models is possible. Short of this, a parametric study was conducted to evaluate the use of more frequent adjustments of empirical parameters. The high quality and density of the SLR and DORIS tracking data sets allow for frequent adjustment of empirical parameters which could, in turn, reduce the orbit error due to dynamic mismodeling. This same philosophy is the hallmark of the reduced dynamic approach used with the GPS tracking data. Therefore, following the study, a new parameterization adjusting drag coefficients C_D every 8 hours, rather than daily constant along-track terms, in addition to the daily along-track and cross-track 1 cpr terms was adopted.

Table 14 demonstrates that the data-weighting change alone had minimal impact on the orbit statistics, whereas the 8-hour drag coefficient empirical parameterization has a more profound effect. However, in combination, the modifications resulted in even better data fits and lower orbit differences.

5.11. Combined Effects of Model Improvements

The effects of changes and improvements in the gravity field model, tide model, nonconservative model, data-weighting, and empirical parameterizations have each been discussed individually. The next logical step was to incorporate all these improvements together, reprocess the POEs (termed the second-generation POEs), and compare them against the GPS orbits. Results are displayed in Table 15, Plates 3c and 4c, and Figure 4c. There are only weak correlations between these improvements in terms of their effect on the orbit differences, and therefore the results are similar to those obtained for the individual cases.

After adoption of these models, agreement with the GPS orbit is now limited by a cycle specific offset in the Z direction (Figure 7). Note that the modeling changes associated with the second-genera-

tion POEs only drop the mean value of the offset from 2.9 to 2.8 cm, with the majority of the impact occurring between cycles 36 and 44. If this mean bias is removed from each cycle, the POE and GPS orbits show remarkable agreement (Table 15, Plates 3d and 4d, and Figure 4d). Power in the major 1 cpr term is reduced by 50% to 1 cm, and the geographically correlated error structure is greatly simplified.

These combined improvements to the POE modeling clearly result in closer agreement with the GPS orbits. This is not to say, however, that the GPS orbits themselves cannot be improved. Accordingly, JPL has also released a limited set of second-generation GPS ephemerides [J. Guinn, personal communication, 1995]. These new orbits incorporate JGM-3, improved tides, and a reference frame more consistent with ITRF. The convergence between the POE and GPS solutions is striking (Table 16). The Z bias, however, remains largely unchanged, and investigations are currently underway to characterize and find its source.

6. Conclusion

Orbit error characteristics in the T/P POEs have been assessed through analysis of SLR residuals and comparisons with the independently determined GPS ephemerides. These have been compared against known and suspected error sources. Omission and commission in the ocean tide model cause the most noteworthy errors and lead to 2- to 3.5-cm amplitude peaks at 60-day periods at fixed geographic locations. Using the power of the GPS data to further "tune" the gravity field, JGM-3 also significantly reduces the orbit error. Nonconservative force modeling does not benefit substantially from the use of telemetered spacecraft information. However, the estimation of additional empirical accelerations at more frequent intervals, as in the GPS orbit solution, does absorb some of the error signal, especially in conjunction with an increase of the SLR data weight with respect to DORIS.

All of these changes, as summarized in Table 17, have been incorporated into a second generation of orbit ephemerides, which will be released on the updated mission GDRs in the fall of 1995. The first- and second-generation POE temporal and spatial orbit error characteristics, as manifested in orbit differences with respect to GPS, are summarized in Table 18. An updated orbit error budget is shown in Table 19. Overall, the 3- to 4-cm radial orbit error for T/P ephemerides on the first-generation GDRs is reduced to below 3 cm for the second generation orbits. The Z bias remains the largest single unexplained phenomenon and is currently the limiting factor in the POE versus GPS orbit comparisons.

Current radial orbit errors are well below the 13-cm mission

requirement. This is accomplished through phenomenal improvement in all facets of orbit determination technology and, especially, in gravity field modeling. Gravity error contributions have dropped by a factor of 30 since the early 1980s. This achievement has identified weaknesses in other models and has driven corresponding improvements. Today, both conservative and nonconservative force model errors are of the same order of magnitude. Further improvement requires intensive efforts in several arenas. Major progress in the gravity field will only be accomplished through a dedicated scientific mission. Tide models will continue to evolve as further altimetry data from T/P and other altimetric spacecraft is reduced. Nonconservative force model errors will be attacked through (1) more detailed and accurate force modeling, limited in scope by the computational burden of evaluating finite element analysis of the spacecraft in near real time, and (2) refinements in the GPS capabilities, such as knowledge of the GPS satellite locations and receiver electronic phase centers. Finally, the Z bias can best be studied through simultaneous processing of the SLR, DORIS, and GPS data types in a single orbit determination software package. This will mitigate any differences arising from tools used for the orbit determination and will assist in defining a single reference frame applicable to all three data types. Although the goal of less than 1-cm radial rms orbit error is not currently attainable, these outlined improvements should bring the T/P orbit error very close to this level.

References

- Antreasian, P. G., and G. W. Rosborough, Prediction of radiant energy forces on the TOPEX/POSEIDON spacecraft, *J. Spacecr. Rockets*, 29(1), 81-90, 1992.
- Bertiger, W. I., et al., GPS precise tracking of TOPEX/POSEIDON: Results and implications, *J. Geophys. Res.*, 99(C12), 24,449-24,464, 1994.
- Bettadpur, S. V., and R. J. Eanes, Geographical representation of radial orbit perturbations due to ocean tides: Implications for satellite altimetry, *J. Geophys. Res.*, 99(C12), 24,883-24,894, 1994.
- Boucher, C., and Z. Altamimi, ITRF 89 and other realizations of the IERS Terrestrial Reference System for 1989, *IERS Tech. Note 6*, Obs. of Paris, April 1991.
- Casotto, S., Ocean tide models for TOPEX precision orbit determination, *Publ. CSR-89-4*, Cent. for Space Res., Univ. of Tex. at Austin, December 1989.
- Chelton, D.B., and M.G. Schlax, Spectral characteristics of time-dependent orbit errors in altimeter height measurements, *J. Geophys. Res.*, 98(C7), 12,579-12,600, 1993.
- Cheney, R.E., J.G. Marsh, and B.D. Beckley, Global mesoscale variability from repeat tracks of SEASAT altimeter data, *J. Geophys. Res.*, 88, 4343-4353, 1983.
- Cheng, M.K., C.K. Shum, R.J. Eanes, B.E. Schutz, and B.D. Tapley, Long-period perturbations in Starlette orbit and tide solution, *J. Geophys. Res.*, 95(B6), 8723-8736, 1990.
- Christensen, E.J., B.J. Haines, K.C. McColl, and R.S. Nerem, Observations of geographically correlated orbit errors for TOPEX/POSEIDON using the global positioning system, *Geophys. Res. Lett.*, 21(19), 2175-2178, 1994.
- Christodoulidis, D.C., D.E. Smith, R.G. Williamson, and S.M. Klosko, Observed tidal braking in the Earth/Moon/Sun system, *J. Geophys. Res.*, 93(B6), 6216-6236, 1988.
- Colombo, O., The dynamics of GPS orbits and the determination of precise ephemerides, *J. Geophys. Res.*, 94(B7), 9167-9182, 1989.
- Colombo, O.L., Altimetry, oceans, and tides, *NASA Tech. Memo*, 86180, 1984.
- Colombo, O.L., Ephemeris errors of GPS satellites, *Bull. Geod.*, 60, 64-84, 1986.
- Cretaux, J.F., F. Nouël, C. Valorge, and P. Janniere, Introduction of empirical parameters deduced from the Hill's equations for satellite orbit determination, *Manuscr. Geod.*, 19, 135-156, 1994.
- Engelis, T., Global circulation from SEASAT altimeter data, *Mar. Geod.*, 9, 1, 45-69, 1985.
- Francis, O., and M. Berge, Estimate of the radial orbit error by complex demodulation, *J. Geophys. Res.*, 98(B9), 16,083-16,094, 1993.
- Guier, W.H., Satellite Geodesy, *APL Tech. Dig.*, 4(3), 2-12, 1965.
- Haines, B.J., G.H. Born, G.W. Rosborough, J.G. Marsh, and R.G. Williamson, Precise orbit computation for the GEOSAT Exact Repeat Mission, *J. Geophys. Res.*, 95(C3), 2871-2885, 1990.
- Haines, B.J., G.H. Born, R.G. Williamson, and C.J. Koblinsky, Application of the GEM-T2 gravity field to altimetric satellite orbit computation, *J. Geophys. Res.*, 99(C88), 16,237-16,254, 1994.
- Kaula, W., *Theory of Satellite Geodesy*, Blaisdale, Waltham, Mass., 1966.
- Lerch, F.J., S.M. Klosko, and G.B. Patel, Gravity model development from Lageos, *Geophys. Res. Lett.*, 9(11), 1263-1266, 1982.
- Lerch, F.J., R.S. Nerem, B.H. Putney, S.M. Klosko, G.B. Patel, R.G. Williamson, H.B. Iz, J.C. Chan, and E.C. Pavlis, Improvements in the accuracy of the Goddard Earth Models (GEM), in *Contributions of Space Geodesy to Geodynamics: Earth Dynamics, Geodyn. Ser.* vol. 24, edited by D. E. Smith and D. L. Turcotte, pp. 191-212, AGU, Washington D.C., 1993a.
- Lerch, F.J., R.S. Nerem, D.S. Chinn, J.C. Chan, G.B. Patel, and S.M. Klosko, New error calibration tests for gravity models using subset solutions and independent data: Applied to GEM-T3, *Geophys. Res. Lett.*, 20(2), 249-252, 1993b.
- Lerch, F. J., et al., A geopotential model from satellite tracking, altimeter, and surface gravity data: GEM-T3, *J. Geophys. Res.*, 99(B2), 2815-2839, 1994.
- Marsh, J.G., and R.G. Williamson, Precision orbit analyses in support of the SEASAT altimeter experiment, *J. Astronaut. Sci.*, 28(4), 345-369, 1980.
- Marsh, J.G., et al., A new gravitational model for the Earth from satellite tracking data: GEM-T1, *J. Geophys. Res.*, 93(B6), 6169-6215, 1988.
- Marsh, J.G., et al., The GEM-T2 gravitational model, *J. Geophys. Res.*, 95(B13), 22,043-22,070, 1990.
- Marshall, J. A., and S. B. Luthcke, Modeling radiation forces acting on TOPEX/POSEIDON for precision orbit determination, *J. Spacecr. Rockets*, 31(1), 89-105, 1994a.
- Marshall, J.A., and S.B. Luthcke, Radiative force model performance for TOPEX/POSEIDON orbit determination, *J. Astronaut. Sci.*, 42(2), 229-246, 1994b.
- Marshall, J.A., S.B. Luthcke, P.G. Antreasian, and G.W. Rosborough, Modeling radiation forces acting on TOPEX/POSEIDON for precision orbit determination, *NASA Tech. Memo.*, 104564, 1992.
- Melvin, P.J., Satellite geodesy from Orlov's plane, *Adv. Astronaut. Sci.*, 65, 1449-1472, 1988.
- Nerem, R. S., B. H. Putney, J. A. Marshall, F. J. Lerch, E. C. Pavlis, S. M. Klosko, S. B. Luthcke, G. B. Patel, R. G. Williamson, and N. P. Zelensky, Expected orbit determination performance for the TOPEX/POSEIDON mission, *IEEE Trans. Geosci. Remote Sens.*, 31(2), 1993.
- Nerem, R. S., et al., Gravity model development for TOPEX/POSEIDON: Joint Gravity Models 1 and 2, *J. Geophys. Res.*, 99(C12), 24,421-24,447, 1994.
- Nouël, F., et al., Precise Centre National d'Etudes Spatiales orbits for TOPEX/POSEIDON: Is reaching 2 cm still a challenge?, *J. Geophys. Res.*, 99(C12), 1994.
- Putney, B. H., et al., Precise orbit determination for the TOPEX/POSEIDON mission, Proceedings of AAS/AIAA Astrodynamics Specialist Conference, *Publ. AAS 95-577*, Am. Astron. Soc., Victoria, B.C., August 1993.
- Ray, R.D., B.V. Sanchez, and D.E. Cartwright, Some extensions to the response method of tidal analysis applied to TOPEX/POSEIDON altimetry (abstract), *Eos, Trans. AGU*, 75(16) Spring Meet. suppl., 108, 1994.
- Rosborough, G.W., Analysis of the JPL and GSFC TOPEX/POSEIDON orbits, memorandum, Goddard Space Flight Center, Greenbelt, Md, December 1993.
- Rosborough, G.W., and B.D. Tapley, Radial, transverse and normal orbit perturbations due to the geopotential, *Celest. Mech.*, 40, 409-421, 1987.
- Rowlands, D.D., J.A. Marshall, J.J. McCarthy, S. Rowton, D. Moore, D.E. Pavlis, S.B. Luthcke, and L.S. Tsaoussi, GEODYN II system description, vol. 1-5, contractor report, Hughes STX Corp., Greenbelt, Md, 1994.
- Schrama, E. J. O., Some remarks on several definitions of geographically correlated orbit errors: Consequences for satellite altimetry, *Manuscr. Geod.*, 17, 282-294, 1992.
- Schrama, E.J.O., and R.D. Ray, A preliminary tidal analysis of TOPEX/POSEIDON altimetry, *J. Geophys. Res.*, 99, 24,799-24,808, 1994.
- Schutz, B.E., and B.D. Tapley, Orbit accuracy assessment for SEASAT, *J. Astronaut. Sci.*, 28(4), 371-390, 1980.
- Schwiderski, E.W., Atlas of the ocean tidal charts and maps, part 1: The semidiurnal principal lunar tide M_2 , *Mar. Geod.*, 6, 4, 1983.

- Tapley, B.D., and G.W. Rosborough, Geographically correlated orbit error and its effect on satellite altimeter missions, *J. Geophys. Res.*, 90(6), 11,817-11,831, 1985.
- Tapley, B.D., et al., Precision orbit determination for TOPEX/POSEIDON, *J. Geophys. Res.*, 99(C12), 24,333-24,404, 1994a.
- Tapley, B.D., et al., The JGM-3 gravity model, *Ann. Geophys.*, 12, suppl. 1, C192, 1994b.
- Wagner, C.A., Radial variations of a satellite orbit due to gravitational errors: Implications for satellite altimetry, *J. Geophys. Res.*, 90(B4), 3027-3036, 1985.
- Wagner, C.A., Geopotential orbit variations: Application to error analysis, *J. Geophys. Res.*, 92(B8), 8136-8146, 1987.
- Wahr, J.M., The tidal motions of a rotating, elliptical, elastic and oceanless Earth, Ph.D. dissertation, University of Colorado, Boulder, 1979.
- Wahr, J.M., Body tides on an elliptical rotating, elastic and oceanless Earth, *Geophys. J. R. Astron. Soc.*, 64, 677-703, 1981.
- Wells, D.E., and P. Vanicek, Least squares spectral analysis, *Rep. BI-R-78-8*, Bedford Inst. of Oceanogr., Dartmouth, Nova Scotia, 1978.
- Wu, S. C., T.P. Yunck, and C. L. Thornton, Reduced-dynamic technique for precise orbit determination of low earth satellites, *J. Guid. Control Dyn.*, 14, 24-30, 1991.
- Yunck, T. P., S. C. Wu, J. T. Wu, and C. L. Thornton, Precise tracking of remote sensing satellites with the Global Positioning System, *IEEE Trans. Geosci. Remote Sens.*, 28(1), 108-116, 1990.
- Yunck, T. P., W. I. Bertiger, S. C. Wu, Y. Bar-Sever, E. J. Christensen, B. J. Haines, S. M. Lichten, R. J. Muellerschoen, Y. Vigue, and P. Willis, First assessment of GPS-based reduced dynamic orbit determination on TOPEX/POSEIDON, *Geophys. Res. Lett.*, 21(7), 541-544, 1994.
- D.S. Chinn, S.M. Klosko, S.B. Luthcke, K.E. Rachlin, R.G. Williamson, and N.P. Zelensky, Hughes STX Corporation, 7701 Greenbelt Road, Suite 400, Greenbelt, MD 20770.
- J.A. Marshall, Space Geodesy Branch, NASA Goddard Space Flight Center, Code 926, Greenbelt, MD 20771.

(Received December 7, 1994; revised June 14, 1995; accepted June 14, 1995.)